

AD-A276 229



2

RL-TR-93-228
Final Technical Report
December 1993



MICROFORCES IN ELECTROMIGRATION

University of Wisconsin
Richard S. Sorbello



DTIC QUALITY INSPECTED 2

APPROVED FOR PUBLIC RELEASE; DISTRIBUTION UNLIMITED.

5480 94-06487

Rome Laboratory
Air Force Materiel Command
Griffiss Air Force Base, New York

94 2 25 231

This report has been reviewed by the Rome Laboratory Public Affairs Office (PA) and is releasable to the National Technical Information Service (NTIS). At NTIS it will be releasable to the general public, including foreign nations.

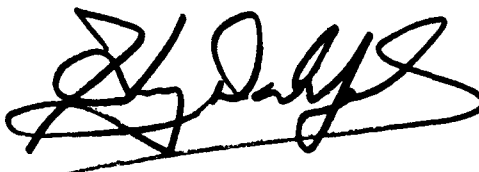
RL-TR-93-228 has been reviewed and is approved for publication.

APPROVED:



MARK W. LEVI
Project Engineer

FOR THE COMMANDER



HARVEY D. DAHLJELM, Colonel, USAF
Director, Reliability
Electromagnetics and Reliability Dir

If your address has changed or if you wish to be removed from the Rome Laboratory mailing list, or if the addressee is no longer employed by your organization, please notify RL (ERDR) Griffiss AFB NY 13441. This will assist us in maintaining a current mailing list.

Do not return copies of this report unless contractual obligations or notices on a specific document require that it be returned.

REPORT DOCUMENTATION PAGE

Form Approved
OMB No. 0704-0188

Public reporting burden for this collection of information is estimated to average 1 hour per response, including the time for reviewing instructions, searching existing data sources, gathering and maintaining the data needed, and completing and reviewing the collection of information. Send comments regarding this burden estimate or any other aspect of this collection of information, including suggestions for reducing this burden, to Washington Headquarters Services, Directorate for Information Operations and Reports, 1215 Jefferson Davis Highway, Suite 1204, Arlington, VA 22202-4302, and to the Office of Management and Budget, Paperwork Reduction Project (0704-0188), Washington, DC 20503.

1. AGENCY USE ONLY (Leave Blank)		2. REPORT DATE December 1993	3. REPORT TYPE AND DATES COVERED Final Sep 89 - Oct 92	
4. TITLE AND SUBTITLE MICROFORCES IN ELECTROMIGRATION			5. FUNDING NUMBERS C - F30602-89-C-0211 PE - 61102F PR - 2306 TA - J4 WU - 24	
6. AUTHOR(S) Richard S. Sorbello			8. PERFORMING ORGANIZATION REPORT NUMBER N/A	
7. PERFORMING ORGANIZATION NAME(S) AND ADDRESS(ES) University of Wisconsin, Milwaukee Dept of Physics Milwaukee WI 53201			10. SPONSORING/MONITORING AGENCY REPORT NUMBER RL-TR-93-228	
9. SPONSORING/MONITORING AGENCY NAME(S) AND ADDRESS(ES) RL (ERDR) 525 Brooks Road Griffiss AFB NY 13441-4505 AFOSR/NE Bolling AFB Washington DC 20332			11. SUPPLEMENTARY NOTES Rome Laboratory Project Engineer: Mark W. Levi/ERDR/(315) 330-2075	
12a. DISTRIBUTION/AVAILABILITY STATEMENT Approved for public release; distribution unlimited.			12b. DISTRIBUTION CODE	
13. ABSTRACT (Maximum 200 words) Theoretical description of electromigration (EM) in metallic microstructures. How EM in a small metallic system is affected by surfaces, interfaces, and extended defects e.g. grain boundaries and dislocations. Electronic aspects of EM and dynamical atom response to current; emphasizing mesoscopic systems. Calculated local transport field in very small structures: near grain boundary or dislocation; and probeability by scanning tunneling microscope. Investigated inelastic scattering effects on electrical conductivity and EM of migrating impurity. Pauli-blocking effects induce non-linearities in the electron and atom response. Mesoscopic systems show this more strongly than bulk systems because Fermi-distribution can be strongly perturbed in state with current. Investigated impurity heating by electron current, quantum-mechanical dynamics of interacting atom-lattice-electron system included; found effective temperature as function of time Net atom flux expressed in terms of effective driving force in Nernst-Einstein relation; in phonon-assisted diffusion of light interstitials driving force can be much smaller than from previous theories. Generalization to non-adiabatic effects on electron screening and direct force for EM. Investigated dynamics in complementary classical diffusion processes; First numerical simulations of atomic level EM. Significant enhancement of light interstitial EM from				
14. SUBJECT TERMS Electromigration, Quantum Mechanics, Mesoscopic, Transport Fields			15. NUMBER OF PAGES 56	
			16. PRICE CODE	
17. SECURITY CLASSIFICATION OF REPORT UNCLASSIFIED	18. SECURITY CLASSIFICATION OF THIS PAGE UNCLASSIFIED	19. SECURITY CLASSIFICATION OF ABSTRACT UNCLASSIFIED	20. LIMITATION OF ABSTRACT UL	

UNCLASSIFIED

13. ABSTRACT (Continued).

dynamical recoil. EM failure times can be much larger than predicted by models neglecting lattice diffusion in completely passivated films with normal operating conditions. Low lattice diffusivity reduces flux of matter leaving grain boundary network during void growth.

UNCLASSIFIED

TABLE OF CONTENTS

Abstract	2
I. Introduction	3
II. Local Transport Field, Electromigration and Residual Resistivity Fluctuations	5
III. STM as a Probe of the Local Transport Field.	7
IV. Current Concentration and Electromigration in a Mesoscopic Point Contact	9
V. Inelasticity, Conductivity and Local Heating in Mesoscopic Systems	11
A. Inelastic Scattering and Electrical Conductivity	12
B. Inelastic Scattering and Local Heating	16
VI. Quantum Theory of Phonon-Assisted Electromigration	20
VII. Numerical Simulations and Dynamical Effects in Electromigration.	24
VIII. Electromigration-Induced Failure and MTF for Metallizations	28
IX. Conclusion	34
References	36
Figure Captions	38
Figures	40

Accession For	
NTIS CRA&I	<input checked="" type="checkbox"/>
DTIC TAB	<input type="checkbox"/>
Unannounced	<input type="checkbox"/>
Justification	
By	
Distribution/	
Availability Codes	
Dist	Avail and/or Special
A-1	

ABSTRACT

A theoretical description of electromigration in metallic microstructures has been developed. We have addressed the question of how electromigration in a small metallic system is affected by surfaces, interfaces, and extended defects such as grain boundaries and dislocations. The electronic aspects of electromigration and the dynamical response of an atom to the electron current have been considered, with special emphasis on mesoscopic systems. In the standard adiabatic picture, the driving force for electromigration is due to the action of the local electric field accompanying the electronic conduction process. We have investigated this local transport field in very small structures, and have calculated the variations of this field in the vicinity of a grain boundary and dislocation. We have found that the spatial variation of this field can be effectively probed by the scanning tunneling microscope. We have also considered the effects of inelastic scattering on the electrical conductivity and on electromigration of a migrating impurity. We find that Pauli-blocking effects due to the exclusion principle give rise to nonlinearities in the electron and atom response with applied voltage. Mesoscopic systems show this effect more strongly than do bulk systems because in mesoscopic systems the Fermi-distribution can be strongly perturbed in the current carrying state. We have investigated the local heating of an impurity by an electron current. Explicit expressions are found for the effective temperature of the impurity as a function of time in the presence of electron and phonon coupling to the impurity. We have performed the first electromigration calculation in which the quantum-mechanical dynamics of the interacting atom-lattice(phonon)-electron system is taken into account. Our theory is most applicable to the migration of light interstitials in metals. We find that the net atom flux can be expressed in terms of an effective driving force according to a Nernst-Einstein relation, but in the case of phonon-assisted diffusion of light interstitials, the driving force can be much smaller than obtained from previous theories. The results have been generalized to account for non-adiabatic effects on electron screening and on the direct force for electromigration. We have also investigated dynamical aspects of diffusion for the complementary case of classical diffusion processes, and we have set up the first numerical simulations of electromigration at the atomic level. We find that for the case of light interstitials, there is a significant enhancement of electromigration due to the dynamical recoil effect. The problem of electromigration-induced failure in metallizations has also been addressed. We show that in completely passivated films operating under normal operating conditions, a bottleneck effect arises due to the low lattice diffusivity, which reduces the flux of matter leaving a grain boundary network during void growth. As a result, typical failure times can be orders of magnitude larger than predicted by models that neglect lattice diffusion.

I. INTRODUCTION

The purpose of our research program was to obtain a better understanding of electromigration in metallic microstructures, with special emphasis on microscopic driving forces and mesoscopic systems. The primary focus of the project is the role of electron current and electric fields on the migration of impurities in metallic microstructures. There are two related aspects to this problem: First, how is a microscopic electric field and microscopic electron current set up in the vicinity of an impurity in a microstructure or a mesoscopic system; and second, how does the microscopic field and current influence impurity migration. In studying this problem it is essential to understand the role of elastic and inelastic electron scattering, both on the electrons and on the impurity.

The study of electromigration in mesoscopic systems is especially useful, both in its own right and for the light it sheds on the physics underlying the electromigration process in a variety of different systems. The crucial aspect of mesoscopic systems is that they have one or more dimensions that are comparable to, or less than, the inelastic mean-free-path. Since the physics of the electromigration process always takes place on this very local, microscopic level, it follows that mesoscopic systems are ideally suited for electromigration investigations. Such phenomena as elastic and inelastic scattering and the close-in dynamics of the coupled impurity-lattice system are natural points of focus in a mesoscopic system. Furthermore, as the dimensions of fine metallic lines become progressively smaller with increased miniaturization, devices in fact, will be entering the mesoscopic regime. At lower temperatures one is in fact already in the mesoscopic regime for some of the very thin films currently in use in integrated circuits.

Building on our previous work,^{1,2} we have investigated the local transport field in the vicinity of an impurity. The local transport field is the microscopic electric field which is dynamically set-up as electrons flow past scatterers in a metallic system. The importance of this field is that it supplies the adiabatic force that drives the atom in the electromigration process. The local transport field arises self-consistently from electron scattering by an impurity (or by any defect for that matter) and the resulting electron pile-up in the vicinity of the scatterer. Because local fields give rise to a change in the voltage across the system, the electrical conductivity of the system is also affected, and this establishes a connection between the electrical conductivity and the driving force for electromigration. The results of some calculations for an impurity near a grain boundary and near a dislocation core are obtained in Section II. The question of whether the local field can be directly probed by means of a scanning tunneling microscope (STM) is addressed in Section III. The results in Sections II and III generalize and extend the results we have reported previously.¹⁻³

An interesting feature of current flow at the microscopic level is that in the vicinity of a scatterer the current flow is inhomogeneous even if the system is macroscopically homogeneous (e.g., a system containing uniformly distributed interstitial impurities or vacancies). Furthermore, in a mesoscopic system such as a "point contact," the current inhomogeneity can extend over very large distances. As a result, there are some novel effects associated with electromigration in these systems. This is shown in Section IV.

A critical aspect of electrical conductivity and electromigration in mesoscopic systems is the role of inelastic scattering of electrons by an impurity and the concomitant local heating that takes place. This is analyzed in Section V. Among the important issues addressed there are the role of the Pauli exclusion principle and the relative importance of energy transfer *vs.* momentum transfer to an impurity that is bombarded by an electron current. The local heating of an impurity by an electron gas is of great importance because it is the mechanism by which a "cold" atom is able to be excited out of its potential well and successfully complete a jump to a neighboring site. In this sense there is no diffusion or electromigration without local heating, or at least, local energy transfer.

Although it is customary to analyze electromigration within a classical description of atom dynamics, there are cases in which the classical picture is inadequate and needs to be replaced by a quantum-mechanical one. An example of this is the electromigration of light interstitial impurities (such as hydrogen in metals) where the atomic jump mechanism is phonon-assisted tunneling. For this mechanism, we have performed a self-consistent quantum mechanical theory of electron screening and non-adiabatic effects in electromigration. This is described in Section VI.

The dynamics of an impurity being subjected to inelastic scattering by an incident electron current is a difficult problem to solve analytically. In the usual adiabatic picture, the collisions are regarded as perfectly elastic and one focuses on the momentum transfers per second to the impurity; this is the so-called "electron wind force." However, it is actually the energy transfer to the impurity that is crucial in exciting an atom out of its potential well. (This conclusion is in keeping with our earlier discussion of the local heating phenomenon, which will be considered in Section V.) The recoil energy effects associated with inelastic scattering go beyond the standard adiabatic picture, and are expected to lead to substantial enhancement of electromigration, especially for lighter atoms. We have investigated the recoil-enhanced electromigration phenomenon by performing numerical simulations for an atom in a periodic potential. The atom is subjected to random collisions with electrons and with a structureless phonon-bath. The impulses from the electron collisions are responsible for the net atomic migration, and the results for light impurities

do show substantial enhancement of electromigration compared to the standard adiabatic model. This work is described in Section VII.

Finally, we investigated electromigration-induced failure and the reliability of metalizations in integrated circuits. Unlike the other work described in this report, which is concerned with the origin of microforces in electromigration, in this reliability study we assumed that a driving force exists and can be described by an effective valence Z^* . We set out to obtain an expression for the mean-time to failure (MTF) for a passivated thin film in the DC regime. By assuming an ideal passivation layer that remains intact, we are able to derive an analytical expression for the MTF. Our result shows that the MTF is greatly increased due to a "bottleneck effect" caused by the requirement that void formation at a grain-boundary triple-point requires vacancies to diffuse out of the grain boundary into the lattice. The MTF analysis is presented in Section VIII.

II. LOCAL TRANSPORT FIELD, ELECTROMIGRATION AND RESIDUAL RESISTIVITY FLUCTUATIONS

Work has been completed on calculating the residual resistivity and electromigration driving force for an impurity near a grain boundary and for an impurity near a dislocation within a jellium model. Previously we had considered these two problems for the case that the electron current is parallel to the plane of the grain boundary and parallel to the axis of the dislocation.¹ We found that in the parallel-current geometry, the impurity feels an electron wind force, $\vec{F}_w(\vec{R})$, which is proportional to the product of the incident electron current and the residual resistivity of the defect complex (impurity plus grain boundary or dislocation).¹ We also showed that $\vec{F}_w(\vec{R})$ correlated well with the *microscopic* current density at the position of the impurity. Hence the electron wind force, is a measure of the local electron "wind." It was found that $\vec{F}_w(\vec{R})$ is smaller when the impurity is inside the grain boundary or dislocation core, essentially because the impurity is shielded from the incident electron current in that case. When an impurity jumps into and out of the grain boundary or dislocation core, fluctuations on the order of 20%–50% are expected in the magnitude of the wind force and in the residual resistivity of the defect complex. Fluctuations of the residual resistivity on this scale would lead to $1/f$ -noise that is compatible with experimentally observed values.⁶ The relevance of our analysis to the experiment is limited, however, because it is restricted to the parallel-current orientation, and in this orientation the extended defect is not effective in scattering electrons.

To overcome this restriction, we have generalized the analysis to include the case that the electron current is perpendicular to the plane of the extended defect, i.e., perpendicular to the grain boundary or parallel to the axis of the dislocation. The perpendicular

orientation is more difficult to treat than the parallel orientation because there is no net momentum transfer to the extended defect in the parallel orientation. Consequently one must employ more drastic approximations to deal with the perpendicular orientation and the associated interference terms between the impurity and the extended defect. To obtain analytic expressions we employ the Born approximation, treating both impurity and extended defect as weak scatterers. (For the parallel orientation, we were able to employ the distorted-wave Born approximation which treats the impurity as a weak scatterer, but the extended defect is treated as an arbitrarily strong scatterer.)

To calculate the wind force and residual resistivity, we use the Born approximation for electron scattering by the net potential $v + U$ where v is the impurity potential and U is the barrier potential associated with the grain boundary or dislocation core. The total wind force \vec{F}_w^{total} on the entire scattering complex can be found from the rate of momentum transfer from the electrons to the scattering complex. This gives

$$\vec{F}_w^{total} = \hbar \sum_{kk'} (\vec{k} - \vec{k}') P_{kk'} g_k,$$

where $P_{kk'} = 2\pi\hbar^{-1} |v_{kk'} + U_{kk'}|^2 \delta(\epsilon_k - \epsilon_{k'})$ is the transition rate between electron states k and k' , corresponding to electron energies ϵ_k and $\epsilon_{k'}$, respectively. The incident shifted electron distribution function is denoted as g_k . The calculation is further simplified by taking the impurity potential to be a very localized s-wave scatterer (delta-function potential).

The total wind force is proportional to the net resistivity presented by the scattering complex.⁴ Using this fact and observing that the interference contribution to the net force arising from the cross-term $v_{kk'} U_{kk'}^*$ is equally shared by the impurity and the grain boundary (or dislocation core), we are able to derive expressions for the wind force and the residual resistivity when the impurity is at position \vec{R} . We find that the part of the residual resistivity that depends upon the position of the impurity is directly proportional to that portion of the wind-force on the impurity that depends upon the position of the impurity. Thus, if we write the resistivity of the system of an impurity in the vicinity of a grain boundary as $\rho(\vec{r}) = \rho_0 + \rho_{GB} + \rho_{imp} + \Delta\rho(\vec{r})$, where ρ_0 is due to thermal phonons, ρ_{GB} is the residual resistivity due to the grain-boundary defect and ρ_{imp} is the residual resistivity due to an impurity in a bulk homogeneous system, then the extra resistivity $\Delta\rho(\vec{R})$, which contains all the dependence of ρ on impurity position \vec{R} , is related to the spatially-dependent part of the wind-force, $\Delta F_w(\vec{R})$, according to $\Delta\rho(\vec{R})/\rho_{imp} = \frac{1}{2} \Delta F_w(\vec{R})/F_w$, where F_w is the wind-force on the impurity in a bulk homogeneous system. (When the impurity is very far from the grain boundary, $\Delta\rho(\vec{R})$ and $\Delta F_w(\vec{R})$ approach zero.)

We have performed detailed numerical calculations of $\Delta\rho/\rho_{imp}$ and find that as an impurity enters a grain-boundary or enters a dislocation core, $\Delta\rho/\rho_{imp}$ is typically of order unity. Thus large variations in resistivity and electromigration driving forces occur when the current is in the perpendicular orientation. This is similar to the result obtained for the parallel orientation although unlike the situation for that case, $\Delta F_w(\vec{R})$ does not correlate with variations in the local current density. It remains true, however, that impurity hopping into and out of an extended structural defect such as a grain-boundary or dislocation can give rise to resistance fluctuations that are compatible with experimentally observed $1/f$ -noise.⁶ Our numerical results for $\Delta\rho(\vec{r})/\rho_{imp}$ in the case of an impurity at position z in the vicinity of a grain boundary is shown in Fig. 1 for different values of the grain-boundary thickness D . In Fig. 2, we show the results for an impurity at position R near a dislocation. In both cases the electron wind is perpendicular to the extended defect (grain boundary or dislocation). We note that when the impurity is within the extended defect, wave-interference of electrons results in an enhancement of $\Delta F_w(\vec{R})$ and $\Delta\rho(\vec{r})$ for repulsive impurity potentials (positive v , or equivalently, negative phase-shift δ_0). On the other hand, suppression occurs for attractive potentials (negative v , or positive δ_0).

III. STM AS A PROBE OF THE LOCAL TRANSPORT FIELD

The local microscopic electric field accompanying electron transport plays a special role in electromigration. This local transport field (LTF) is a local electric potential set up by the pile-up of current carriers in the vicinity of defects when a transport current passes through a conductor.¹⁻⁵ It is the total LTF drop across a sample that contributes to the macroscopic voltage drop across the sample,⁵ and it is the gradient of the LTF that gives a driving force on an impurity within an adiabatic description of electromigration.

It would be very useful if there existed an independent way of measuring the LTF. A possible technique for measuring the LTF in mesoscopic systems would be to probe the system with a scanning tunneling microscope (STM). In such a technique, one could simultaneously measure the surface topography and the spatial variations of the LTF across a grain boundary, for example. The local potential in the sample might then be associated with the measured STM voltage. The validity of this association is not clear. In a previous study^{1,3} we showed that some qualitative features of the LTF could be recorded by the STM. However, in that study we neglected the phase coherence of the scattered electron waves at the grain boundary. We have now included these important interference terms in our analysis.

A theoretical approach was devised to analyze the LTF and the voltage measured by the STM in a current-carrying mesoscopic system. Generalizing our earlier work,³ we

considered the phase coherence between the incident electron wave and the electron wave reflected from a defect. This phase coherence leads to Friedel-like oscillations in both the LTF and STM voltage (V_{STM}). The expressions for the electric potential corresponding to the LTF and to the STM voltage turn out to be formally identical, and have the form⁷:

$$V_{STM}(\vec{r}) = V_{LTF}(\vec{r}) = [\mu_{STM}(\vec{r}) - \mu]/e$$

where μ is the equilibrium chemical potential (in the absence of current) and e is the magnitude of the electron charge. Here $\mu_{STM}(\vec{r})$ is given by the following weighted average of the incident electron distribution, g_{nk} :

$$\mu_{STM}(\vec{r}) = \frac{\sum_{nk} D_{nk} g_{nk}}{\sum_{nk} D_{nk}}$$

where $D_{nk} = |\psi_{nk}(\vec{r})|^2 \delta(\epsilon_{nk} - \mu)$ is a local density of states factor, which depends on the electron scattering wavefunctions ψ_{nk} . The wavefunction quantum numbers n, k refer to transverse modes n perpendicular to the surface and traveling waves of wavevector k parallel to the surface. Despite the formally identical expressions for V_{STM} and V_{LTF} , there is a critical distinction between the two quantities. The point is that the STM picks up the electron wavefunctions at position \vec{r} which is in the vacuum region outside the metal, whereas the LTF picks up the wavefunctions at position \vec{r} which is inside the metal. Now, electron wavefunctions decay exponentially into the vacuum region, with the decay being less rapid for higher modes of the transverse standing wave patterns. Consequently, V_{STM} is being more heavily weighted by the higher-mode electron wavefunctions and does not accurately describe the LTF inside the metal.

To study the accuracy of scanning tunneling potentiometry in measuring the LTF, we calculated the spatial profile of LTF and V_{STM} for the case of grain boundaries in a thin film and for the case of an impurity near a surface. For the case of a thin film containing grain boundaries within the jellium model, we find that V_{LTF} and V_{STM} differ in their spatial variation, but their drops across a grain-boundary are of the same order of magnitude. In general, the V_{STM} fluctuates on a larger length scale than the LTF. The reason for this behavior is that the wavefunctions dominating the STM response have higher transverse momentum and therefore smaller longitudinal momentum. The smaller longitudinal momentum implies variations of longer wavelength. This behavior is illustrated in Fig. 3, where the STM voltage profile and the LTF profile is plotted in a region across a grain boundary in aluminum metal.

For the case of a scatterer on a metal surface, the short range variations of both V_{STM} and V_{LTF} near a surface scatterer are on the order of 1 μ V when the current density is

on the order of 10^7 A/cm and the distance d between the STM tip and the metal surface is about 3 Å. Observation of the long-range variation in V_{STM} away from an impurity requires sub-microvolt resolution and smaller values of d . The results are illustrated in Fig. 4, which shows the V_{STM} and LTF profiles calculated near an impurity at the surface of an aluminum film.

Our general conclusion is that the STM can be profitably used as a qualitative probe of the local transport field in the vicinity of a defect in a mesoscopic system, and that the gradient of this potential field should correlate with the electromigration driving force.

IV. CURRENT CONCENTRATION AND ELECTROMIGRATION IN A MESOSCOPIC POINT CONTACT

Continuing microminiaturization of electronic devices (including nanofabrication) has resulted in increasing interest being attached to mesoscopic systems, i.e., those systems whose dimension along the direction of transport is smaller than the inelastic electron mean free path. Such systems have provided a convenient and powerful instrument for studies of quantum interference phenomena and spectroscopy of elementary excitations in solids. Here we investigate a unique possibility for electromigration studies offered by mesoscopic metal constrictions (point contacts).

When studying electromigration phenomenon one is interested in a microscopic driving force \vec{F} exerted on the impurity atom by the local transport electric field. This force, as well as the field itself, consists of two parts traditionally called the “direct” and the “electron-wind” contributions. The direct force \vec{F}_d is associated with the local electric field \vec{E} existing in the absence of the migrating atom, which is, however, screened to some extent by the polarization of electrons around the impurity. The wind force \vec{F}_w arises from the scattering of the electron flow by the impurity atom. In the simplest case (e.g., free-electron-like system) this force is given by $\vec{F}_w = Ke\vec{j}_e$ where \vec{j}_e is the local electron charge-density current.^{4,8,9} The coefficient K , although its form differs for different microscopic models, is not a point of any serious theoretical disagreement.

As opposed to that, the magnitude of the direct force \vec{F}_d is a subject of long-lasting controversy. A number of authors¹⁰⁻¹² showed that for a weakly scattering impurity the effective screening of its charge due to the polarization of the electron gas is small, i.e., the direct valence Z_d defined by $\vec{F}_d = Z_de\vec{E}$ is close to the bare valence Z . The considerable deviation of Z_d from Z can be caused by strong scattering,¹³⁻¹⁵ there can also be a renormalization due to non-adiabatic electron response.¹⁶ At the same time, according to some other workers' views,^{17,18} weak scatterers as well as strong scatterers are completely screened by conduction electrons, and consequently, $Z_d = 0$.

The main difficulty in the experimental determination of the direct valence is that for a bulk-like system Z_d appears in any measurable characteristic in combination with the electromigration wind-force coefficient K . (By definition, the effective valence due to the wind force Z^*_w , is related to K by $Z^*_w = K/\rho$, where ρ is the sample resistivity). Indeed, if the local Ohm's relation for electrons $\vec{j}_e = \sigma \vec{E}$ holds, then the total driving force can be written as $\vec{F} = Z^* e \vec{E}$ with the so-called effective valence $Z^* = Z_d + K/\rho$. Therefore, the value of Z_d can only be obtained by the insufficiently reliable method of separating a resistivity-independent part of Z^* in electromigration experiments.¹⁹

The situation is quite different in the case of a metal constriction having a dimension, a , smaller than both the elastic and inelastic electron mean free paths, and connecting two bulk samples. In such a system electrons traverse a constriction region along the quasiclassical trajectories ballistically, i.e., without scattering if $a \gg \lambda_F$, where λ_F is electron Fermi wavelength. However, the geometric effect of current concentration is responsible for the large resistance of a ballistic point contact. The resistance is of order $\hbar e^{-2} (\lambda_F/a)^2$ and is determined by the nonequilibrium electron distribution and the transport electric field in the constriction region.^{4,20-22} In this situation a steady state is characterized by $\text{div } \vec{j}_e = 0$, $\text{div } \vec{E} \neq 0$, and consequently, the local Ohm's law relation no longer holds. In this case, the driving force for electromigration has the general form

$$\vec{F} = Z_d e \vec{E} + K e \vec{j}_e$$

and so, an impurity current $\vec{J}_i = N_i M \vec{F}$, determined by atomic mobility M , has a non-conserved ($\text{div } \vec{J}_i \neq 0$) part proportional to the direct valence Z_d . Such nonconservation requires the existence of the diffusive current component $\vec{J}_{dif} = -D \vec{\nabla} N_i$, i.e. a spatially inhomogeneous impurity density N_i , in order for the net current to be conserved. The inhomogeneous part of N_i determines a nonlinear correction to the current-voltage characteristic, associated with scattering of electrons by the impurities. This effect can be used for a direct measurement of Z_d .

We have performed a general analysis of the steady-state electron and impurity transport problem in a mesoscopic point contact. The analysis is based on the simultaneous solution of the kinetic equation for electrons and the continuity equation for both electrons and impurity atoms, with the electroneutrality condition taken into account. As a result, we obtained the general expression for the normalized nonlinear correction I'_e to the I - V characteristic I_e ²³:

$$\frac{I'_e}{I_e} = \gamma \frac{Z_d e V}{k_B T + Z Z_d \bar{N}_i / \nu_F}$$

Here T is the temperature, Z is the bare valence, \bar{N}_i is the equilibrium impurity density, and ν_F is the electron density of states at the Fermi level. The parameter γ depends only on the point contact geometry and on the electron transport regime. For the quasiballistic regime ($\ell_e = v_F \tau > a$) we get an estimate $\gamma \sim a/\ell_i$ with $\ell_i = v_F \tau_i$ being the electron mean-free-path due to impurity scattering. The above relation for I'_e/I_e can be used for a direct determination of Z_d from the I - V characteristic. Assuming temperature-independent Z_d , we get

$$Z_d = -\frac{\nu_F}{Z\bar{N}_i} \left(\frac{I_e^{(2)}}{\partial I_e^{(2)}/\partial T} + k_B T \right),$$

where $I_e^{(2)} = d^2 I_e / dV^2$. Hence, the value of the direct valence can be obtained by measuring the temperature-dependent second derivative of the I - V characteristic of a mesoscopic point contact in the quasiballistic regime. These measurements can be easily done using well-developed point-contact techniques.²⁴

We note that our results are not based on any specific mechanism of atomic diffusion, and are, therefore, quite general. The only restrictions are those of low enough temperature for the inelastic mean free path to be larger than point contact dimension a , and low voltage so that I'_e/I_e be small. These conditions are readily attainable.

V. INELASTICITY, CONDUCTIVITY AND LOCAL HEATING IN MESOSCOPIC SYSTEMS

Inelastic scattering has especially important consequences for electromigration and electron transport in mesoscopic systems. Of specific interest is the question of energy transfer to atoms and the role of the Pauli exclusion principle in blocking transitions of electrons between states. Such effects have been traditionally ignored in electromigration theory, even though it is the very energy transfer to an atom that allows the atom to climb over the barrier and accomplish a diffusion jump. The process by which an atom gains sufficient energy to jump over a potential barrier may be described as "local heating." That is, an initially cold atom is heated, or raised in energy, by interactions with the electron gas and with the lattice atoms (phonons).

The inelastic interaction of an impurity atom with the electron gas is of primary concern. This interaction has two important effects, namely, it modifies the electronic conductivity, and it can excite the atom to a higher effective temperature (local heating effect). To investigate these effects, we consider a simple geometry consisting of an impurity between two electron reservoirs that are kept at different chemical potentials. This is the situation relevant to a very narrow mesoscopic conductor that provides a channel for electrons to flow between two massive voltage pads. We first present an analysis of the

effect of inelastic scattering on the electrical conductivity; after that, we consider the local heating phenomenon.

A. Inelastic Scattering and Electrical Conductivity

The microscopic response of the electron-atom system has been considered within a scattering theory approach.^{25,26} We have investigated the transport of an electron current through a mesoscopic system consisting of a confined electron gas and an impurity, taking into account the energy loss by the electron gas to the impurity. We can thus account for phonon-like excitations of the vibrating or moving impurity and the Pauli-blocking effect caused by the restrictions of the Pauli exclusion principle on electronic transitions. In contrast to previous treatments of inelastic scattering, we focus on the effects due to a single impurity scatterer in a mesoscopic system. The impurity is treated as a dynamical entity which can recoil and transfer energy and momentum to the lattice. In focusing on a single impurity, we are excluding from consideration the multiple scattering of electrons through an array of scatterers or through a random distribution of background inelastic scatterers. In exchange for this simplification, we are able to consider in microscopic detail the effects of a scatterer at which both elastic and inelastic processes can occur. In this respect, the system we consider is the single-impurity realization of Büttiker's model in which a voltage probe simultaneously acts as an elastic and inelastic scatterer.²⁶ We make no *a priori* assumptions, however, concerning the separation of coherent and incoherent processes at the microscopic level.

Within our model of a single dynamical impurity in a mesoscopic system, we assume that the impurity's degrees of freedom are in thermal contact with the solid at constant temperature. When the incident electrons are scattered by the impurity, both elastic and inelastic scattering events are possible. However, it is clear that some inelastic events will be blocked because of Pauli-exclusion restrictions on final electron states. Because of current-conservation, this Pauli-blocking must also have an indirect effect on elastic scattering processes. Furthermore, the effectiveness of Pauli blocking will depend on the energy of the incident electrons with respect to the equilibrium Fermi energy. As a consequence, the electron conductance will be voltage dependent, and a new type of nonlinearity is suggested by our calculations. The nonlinearity arising in our treatment is an inelastic effect and represents the dynamical coupling between the injected current and the impurity. It arises from the fact that only electrons with enough excess energy given by the shift of Fermi level are capable of producing impurity excitations, hence the I-V characteristics become a probe for the dynamical spectrum of the target system and for the scattering mechanism.

Our expression for the current going through a microstructure consisting of a narrow channel connecting two voltage pads, held at voltage difference V with respect to each other, involves an integral over energies E, E' and the dynamic structure factor $S(q, \omega)$. Explicitly, we found²⁷

$$J = \frac{e}{h} \int dE [f(E - eV) - f(E)] \\ - \frac{e}{h} |r|^2 \int dE \int dE' \{ S(2k_F, E - E') f(E - eV) [1 - f(E')] \\ - S(2k_F, E' - E) f(E') [1 - f(E - eV)] \}$$

where $|r|^2 = \left(\frac{m}{\hbar^2 k_F}\right)^2 |V(2k_F)|^2$ is the elastic reflection coefficient for electrons of mass m at the Fermi level, k_F is the Fermi wavevector and $V(2k_F)$ is the scattering potential evaluated for backscattering on the Fermi sea. The blocking effect due to Pauli exclusion is evident from the factor $(1 - f)$, where f is the final state distribution for the electrons. The dynamics of the impurity enter only in the dynamical structure factor $S(q, \omega)$, which depends on the nature of the impurity and on the so-called recoil energy, given by $R = \hbar^2 q^2 / 2M$ for an impurity of mass M . Explicitly, the dynamic structure is defined as follows:²⁸

$$S(q, \omega) = \frac{1}{2\pi\hbar} \int_{-\infty}^{+\infty} dt e^{-i\omega t} \langle e^{-iqX} e^{iqX(t)} \rangle_T$$

where $X(t)$ is the time dependent impurity coordinate in the Heisenberg representation.

Once a model for the impurity scatterer is chosen, $S(q, \omega)$ may be calculated and the results then used in the expression for J . This, in turn, allows us to determine the conductance G , which is defined as dJ/dV . We have initiated such a program for two specific models of an impurity, namely, the harmonic oscillator model and the free-particle model. In terms of the electromigration phenomenon, these cases represent complementary situations—the oscillator model is appropriate for an impurity before it undertakes a diffusion jump, and is more or less rattling around in its cage, while the free particle model is more appropriate to the situation when the impurity is “in flight” between lattice sites. For each case, we were able to determine analytically the dynamic structure factor, and use the results to evaluate our conductance expressions.

For the case of an impurity oscillating in its well, we find that relative to the idealized case of perfectly elastic scattering there is a reduction in the conductance (or an increase in the resistance) due to the motion of the impurity, and this effect is present even in the case of zero-temperature. In the latter case, it is the zero-point motion of the impurity that

accounts for the extra resistance. In general, as the voltage V increases, the conductance G remains flat until an energy is reached where an impurity vibration (localized phonon) can be excited. The condition for this is $eV = \hbar\omega$, where ω is the natural (angular) frequency of oscillation of the impurity in the harmonic-oscillator well. At this value of V , the conductance drops down to a lower value, and stays there as V increases until $eV = 2\hbar\omega$, which corresponds to 2-phonon excitations, and similarly, for n -phonon excitations. We estimate that these nonlinearities would be experimentally measurable for metallic systems containing light interstitial impurities, such as hydrogen. Our numerical calculations for $G(V)$ are shown in Fig. 5 for the case that the impurity is a bound particle oscillating in a well. In Fig. 6 we show results for the case that the impurity is still bound but is now very weakly bound.

For the case that the impurity acts as a free-particle in solid, we find that except for thermal spreading, the scattering of an electron by a free impurity is solely inelastic and is blocked at $V = 0$. The conductance equals e^2/h before eV reaches the recoil energy, at which point it suddenly drops and becomes flat again with increasing V . (The fraction by which the conductance drops is $|r|^2$, where r is the reflection amplitude for elastic scattering). In general, the blocking effect due to the Pauli exclusion principle plays a crucial role: The nonlinear behavior of G is characterized by the opening-up of Pauli-blocked channels at finite voltage. The results for a free-particle impurity are shown in Fig. 7. Note the similarity to the weakly bound case; the distinction in these two cases is that the discrete phonon levels are obliterated, and a smooth continuum of excitations replaces these discrete levels.

We have generalized our theory beyond the quasi 1-dimensional mesoscopic system to treat the case of a 3-dimensional mesoscopic system. In extending our analysis to a 3-dimensional mesoscopic system, we consider a point-contact geometry with a mesoscopic bridge connecting two otherwise separated bulk metals. The mesoscopic structure is taken to be an electron waveguide, with direction of transmission along the z -axis. The cross-section of the waveguide in the xy plane is rectangular with width w and thickness d . The confined electrons have quantized transverse energy levels, each of which is referred to as a channel. As a basic assumption, we adopt the adiabatic flare model²⁹ for the restriction openings, so that the transverse energy levels extend continuously into the region far away from the restriction.

As in our previous studies of an electron waveguide,²⁹ we can write the unperturbed single electron wave function as

$$u_{\mu\nu}(\vec{r}) = \sqrt{\frac{2}{\pi wd}} \sin\left[\frac{\mu\pi x}{d}\right] \sin\left[\frac{\nu\pi y}{w}\right] e^{ikz}$$

where the channel indices μ and ν are positive integers. The energy of an electron with channel indices (μ, ν) and momentum k in the z -direction is $E_{\mu\nu k} = \hbar^2 K^2 / 2m$, where $K^2 = k^2 + (\mu\pi/d)^2 + (\nu\pi/w)^2$.

After some considerable mathematical processing, we can express the conductance G of the system in terms of a generalized dynamical structure factor $S(\vec{q}, \vec{q}'; \omega)$ which contains all the necessary information about impurity dynamics. In the special case of a free-particle impurity, and a conducting channel having dimensions much larger than an electron wavelength, we find that the I-V curve is again non-linear, i.e., G shows significant dependence on V . Our result for this case can be cast into the suggestive form²⁷

$$\frac{1}{e} \frac{dG}{dV} = -\frac{e^2}{4} g(E_F) v_F \left[\frac{d\sigma(\epsilon)}{d\epsilon} - \frac{d\sigma(-\epsilon)}{d\epsilon} \right]_{\epsilon=eV}$$

where $\sigma(\epsilon)$ is the total scattering cross section for electron energy loss less than or equal to ϵ , and $\sigma(-\epsilon)$ is the total scattering cross section for electron energy gain less than or equal to ϵ . Here $g(E_F)$ is the density of states at the Fermi level and v_F is the Fermi velocity.

Similar to what we found for the 1d case, we find that for a free impurity, electron scattering is inelastic; it is therefore blocked when the voltage V equals zero at low temperatures. Therefore the conductance at $V = 0$ equals G_o , which is the conductance in the absence of the impurity, and which is given by

$$G_o = \frac{1}{4} e^2 v_F g(E_F) A$$

with A being the cross-sectional area of the electron waveguide. The above equations specify the entire G - V curve. We find that at sufficiently large voltage ($eV \gg$ Recoil energy) the net drop of conductance due to impurity scattering is given by

$$\frac{\Delta G}{G_o} = \frac{1}{A} [\sigma(\infty) - \sigma(-\infty)].$$

We point out that the nonlinearities which we have obtained here should be directly measurable in nanobridge circuits of the kind investigated by Ralls *et al.*³⁰, and should correlate with electromigration in such systems. In principle, the opening-up of Pauli-blocked channels and the associated non-linearity due to inelastic scattering are also present for bulk systems. However, because of the extremely small drift velocity of the electrons, the effect is negligible in bulk systems even at current densities on the order of 10^6 A/cm². On the other hand, for mesoscopic systems the departure of Fermi level from equilibrium can be substantial, as V can be in the millivolt range or larger. Therefore, the link between inelasticity and nonlinearity is, ultimately, a mesoscopic characteristic.

B. Inelastic Scattering and Local Heating

Inelastic electron scattering of electrons by an impurity will affect the impurity's energy and spatial distribution, and this will be important for electromigration. We have analyzed the thermal excitation of an impurity atom by an electron current in a mesoscopic system. The impurity is taken to be a harmonic oscillator that is only weakly coupled to the electrons and to the phonons. The electrons and the phonons act as thermal baths to the impurity and are treated separately. First we consider the density matrix of the combined system of the electrons and the impurity. Following the Landauer-Büttiker scattering theory formulation for mesoscopic systems,^{25,26} we assume that the incident electron distribution, having temperature and chemical potential determined by the reservoirs, is not affected by the weak electron-impurity interaction. This allows us to "trace out" the electron degrees of freedom and arrive at a master equation for the impurity. The solution to the master equation shows that the current carrying electrons act as a thermal bath for the impurity with an effective temperature determined by the voltage. Thermal heating is given in terms of impurity "relaxation" towards this elevated temperature. Phonons enter into the impurity master equation as an additional term which attempts to bring the impurity back into thermal equilibrium with the lattice.

We consider the probability function for an impurity atom to be at some energy ϵ in its potential well at time t . Denoting this distribution as $P(\epsilon, t)$, we can average over all electron transitions (i.e., "trace-out" the electron degrees of freedom) and obtain

$$\frac{\partial}{\partial t} P(\epsilon, t) = - \sum_{\epsilon'} \{ W(\epsilon', \epsilon) P(\epsilon, t) - W(\epsilon, \epsilon') P(\epsilon', t) \}$$

where $W(\epsilon', \epsilon)$ is the transition rate from state $|\epsilon\rangle$ to state $|\epsilon'\rangle$, and $W(\epsilon, \epsilon')$ refers to the reverse process.

Explicitly evaluating $W(\epsilon', \epsilon)$ using the Born approximation, we get³¹

$$W(\epsilon', \epsilon) = \frac{1}{2\pi\hbar} |r|^2 |\langle \epsilon' | e^{2ik_F X} | \epsilon \rangle|^2 [\beta_e^{-1}(eV + \epsilon - \epsilon') + \beta_e^{-1}(eV - \epsilon + \epsilon') + (\epsilon - \epsilon')]$$

where the function β_e is defined by

$$\beta_e(x) = \beta \frac{\tanh(\beta x/2)}{(\beta x/2)}$$

The dynamical distribution of the inelastic process is governed by the "structure-factor" $|\langle \epsilon' | e^{2ik_F X} | \epsilon \rangle|^2$, where X is the position of the impurity, and $\beta = 1/k_B T$, where T is the equilibrium temperature of the reservoirs and k_B is Boltzmann's constant.

In our subsequent calculations we consider the situation of moderately large voltage bias V , where the effect of Pauli blocking is unimportant and thus the excitation of the impurity by the electrons is fully realized. Since local heating is expected to be most important when the current density at the impurity is high, the high-bias limit is relevant for studying the local heating effect in mesoscopic systems.

Within our model we can obtain analytical results in the high-bias, high temperature regime defined by $eV, k_B T$ much greater than the recoil energy R , which is typically on the order of an meV or less. The result is that if the atom is initially at thermal equilibrium before the electron current is turned on, then the distribution at any later time t is a Boltzmann distribution with a time-dependent temperature, i.e.,³¹

$$P(\epsilon, t) = \beta_t e^{-\beta_t \epsilon}$$

with

$$\beta_t^{-1} = \beta_e^{-1} - (\beta_e^{-1} - \beta^{-1}) e^{-t/\tau_e}$$

where the subscript t in β_t denotes the time variable. The effective temperature $T_{eff}(t)$ is related to β_t in the usual way, namely, $k_B T_{eff}(t) = \beta_t^{-1}$. Note that our expression for β_t^{-1} implies that β_t^{-1} satisfies the equation

$$\dot{\beta}_t^{-1} = -\frac{\beta_t^{-1} - \beta_e^{-1}}{\tau_e},$$

which is a relaxation-rate equation for the temperature. (Here and in what follows, when we refer to β_t^{-1} as temperature, we are using energy units in which $k_B = 1$.) In the above, $\tau_e^{-1} = (R/\pi\hbar)|r|^2$ plays the role of the relaxation rate characterizing the electron-impurity scattering. Using typical values for the recoil energy R and the reflection coefficient r for electron scattering, we estimate that $\tau_e \sim 10^{-10}$ s. This very short time implies that local heating is virtually an instantaneous process. However, this need not be the case when the external driving field (and the associated electron current) is very rapidly oscillating, i.e., for driving frequencies on the order of GHz.

We now turn our attention to the effect of a phonon bath. In general, both non-equilibrium electrons and phonons are coupled to the impurity, and local heating by electrons occurs when the phonon coupling is relatively weak. In that case, the energy deposited at an impurity remains rather well localized in the vicinity of the impurity. On the other hand, if the impurity-phonon coupling is large, most of the energy deposited at the impurity effectively leaks away into the lattice.

To analyze the effect of coupling between the impurity and the phonon bath, we consider an interaction between the impurity and the phonons in the simple form:

$$\sum_k g_k (a_k b^+ + b a_k^+)$$

where g_k is the coupling constant between the impurity and the lattice, b^+ and b are the creation and annihilation operators for impurity oscillations with frequency Ω , and a_k^+ , a_k are the creation and annihilation operator for a lattice phonon with wave vector k . The phonon distribution is given by

$$n(\omega_k) = \langle a_k^+ a_k \rangle = \frac{1}{e^{\beta \hbar \omega_k} - 1}$$

where $\langle \dots \rangle$ denotes the ensemble average, ω_k is the frequency for lattice mode k , and β is the inverse lattice temperature which is taken to be the same as the inverse temperature of the electron reservoirs.

In the first-order Born approximation the transition rate of the impurity due to phonon scattering is given by

$$W(\epsilon', \epsilon) = \frac{2\pi}{\hbar} |\langle \epsilon' | b^+ | \epsilon \rangle|^2 |g(\Omega)|^2 \Gamma(\Omega) n(\Omega) + \frac{2\pi}{\hbar} |\langle \epsilon' | b | \epsilon \rangle|^2 |g(\Omega)|^2 \Gamma(\Omega) [n(\Omega) + 1] \quad (22)$$

where $\Gamma(\Omega)$ is the phonon density of states at $\omega_k = \Omega$, and $|g(\Omega)|^2$ is $|g_k|^2$ averaged over all orientations in k -space at $\omega_k = \Omega$.

For a weakly bound impurity, Ω lies within the spectrum of ω_k , and the impurity forms a resonant mode with a decay rate determined by $W(\epsilon', \epsilon)$. When Ω lies outside the range of ω_k , $W(\epsilon', \epsilon) = 0$, and the impurity gives rise to a localized mode whose lifetime can be calculated provided that there is anharmonic coupling between the impurity and the lattice. In the present work, we consider the case where the impurity is weakly bound and forms a resonant mode. For simplicity we also assume that $\hbar\Omega$ is small in comparison with the experimental temperature β^{-1} .

Following the mathematical steps of our earlier analysis, we are again able to solve the master equation, and we find³¹

$$P(\epsilon, t) = \beta_t e^{-\beta_t \epsilon}$$

with

$$\beta_t^{-1} = \beta_d^{-1} - (\beta_d^{-1} - \beta^{-1}) e^{-t/\tau}$$

where

$$\beta_d^{-1} = \frac{\tau_e \beta^{-1} + \tau_p \beta_e^{-1}}{\tau_e + \tau_p},$$

and $\tau^{-1} = \tau_e^{-1} + \tau_p^{-1}$. The quantity τ_p is the scattering time appropriate to the phonon-impurity interaction, and is given by $\tau_p^{-1} = 2\pi\hbar^{-1}|g(\Omega)|^2\Gamma(\Omega)$. Our result for β_t^{-1} implies that the effective temperature satisfies the new relaxation equation

$$\dot{\beta}_t^{-1} = -\frac{\beta_t^{-1} - \beta_d^{-1}}{\tau} = -\frac{\beta_t^{-1} - \beta_e^{-1}}{\tau_e} - \frac{\beta_t^{-1} - \beta^{-1}}{\tau_p}$$

We conclude that the impurity-phonon coupling provides an additional relaxation term for the impurity's thermal energy. Local heating takes place as the impurity relaxes towards a weighted defect temperature β_d^{-1} at a rate given by τ^{-1} . The dotted curve in Fig. 8 shows β_d^{-1} as a function of eV , with $\tau_p/\tau_e = 0.5$. We see that the defect temperature is lower than the effective electron temperature β_e^{-1} due to coupling to a phonon bath. Generalizations of these results to a 3-d model have been given elsewhere.³¹

We now discuss our results in the light of previous work. For the electron-impurity interaction part, the present work agrees with the steady state numerical calculation of Ralls *et al.*³⁰ in that the non-equilibrium electrons from the shifted Fermi distribution provide a thermal interface to the impurity with an effective temperature higher than the reservoir temperature β^{-1} . Notable in our derivation are the explicit expressions for the two key quantities for understanding local heating, namely, β_e and τ_e , which arise naturally from consideration of the time dependent impurity distribution function. In the presence of a phonon bath, we are able to incorporate the effect of impurity-phonon coupling into the same framework as for the electrons. We thereby arrive at expressions for an asymptotic effective temperature β_d which characterizes the defect coupled both to electrons and phonons. The rate at which the local temperature approaches β_d is governed by the relaxation time τ , which is a function of both τ_e and τ_p . These results are consistent with the model used by Ralls *et al.*³⁰ in explaining their experimental results.

When a current driven by the chemical potential difference eV flows across a mesoscopic system, the effective temperature of the electrons is a fraction of eV on the energy scale. For applied voltages from 10 to 1000 mV, the temperature ranges from 10 to 1000 K. For a quasi-classical metallic point-contact structure, $\tau_e^{-1} \simeq 10^{10} \text{ sec}^{-1}$ for an electron-impurity cross section $\sigma = 1\text{\AA}^2$. Therefore, local heating is effectively an instantaneous process, and is capable of ripping an isolated impurity atom out of its potential well in a very short time. A limitation to such a dramatic effect is due to the impurity-phonon coupling, characterized by the relaxation rate τ_p^{-1} . For strong impurity-phonon coupling,

$\tau_p^{-1} \gg \tau_e^{-1}$, and local heating will be insignificant. On the other hand, when τ_p^{-1} is smaller than or is comparable to τ_e^{-1} , local heating is significant, and one expects to see local heating assisted electromigration at high sample biases. In reference 30, τ_p^{-1} is found experimentally to be comparable to or slightly smaller than τ_e^{-1} , and indeed electromigration resulting in permanent sample resistance change has been deduced from that experiment.

To summarize, we have obtained a solution to the master equation for a single impurity subject to electron and phonon scattering in mesoscopic systems. In the case of high bias and high lattice temperature, we are able to show that the impurity follows a Boltzmann distribution with a time-dependent temperature relaxing towards the steady state local temperature. Hence, in this case local heating and time-dependent temperature are concepts having thermodynamic justification.

VI. QUANTUM THEORY OF PHONON-ASSISTED ELECTRO-MIGRATION

Theoretical work on electromigration in the literature has avoided the central problem of simultaneously describing electron dynamics and impurity dynamics. Invariably, one separates out the role of electrons in causing a driving force and then considers how this driving force affects the impurity motion. We are the first to describe the combined system as a single quantum mechanical entity using the polaron picture for diffusion.³²⁻³⁴ This allows us to avoid some of the questionable assumptions that are implicit in earlier treatments, e.g., adiabaticity of impurity response, neglect of recoil effects, validity of the Nernst-Einstein relation in electromigration, and the passive role of phonons.

The picture which we developed works best for light interstitials. The impurity interacts with all lattice atoms dynamically and with a static substrate potential as well. The electrons interact with the impurity, which is assumed to start off in an interstitial well. The diffusion jump occurs when the lattice atoms vibrate at thermal equilibrium and give rise to a fluctuation that increases the energy of the impurity in the original well thereby making it energetically favorable to make a transition to a neighboring well. The new feature which we are incorporating is the interaction of the impurity with the out-of-equilibrium electron system as well as the usual atomic-polaron interaction between the impurity and the lattice atoms.³²⁻³⁴ We initially focus on the light interstitial impurities, in which case quantum effects are expected to play a very important role.

Generalizing the approach developed in References 32-34 for simple diffusion in the absence of an applied field, we consider weak tunneling between localized states at adjacent interstices as a basic mechanism for atomic transport. Furthermore, we assume sufficiently

strong atom-phonon interaction, rather high temperature and a not extremely low concentration of static lattice defects, which is the typical experimental situation. In this regime the atom band motion is completely destroyed,³³ and the transport occurs by incoherent hopping between polaron-type states at neighboring interstices. We also suppose that the concentration of interstitial impurities under consideration is low enough to neglect the interaction between them and the effects of quantum degeneracy.

As far as electromigration is concerned we consider the effects of both the external electric field acting directly on the impurity and the scattered electron flow. The latter generates a wind force on the interstitial atom during the hopping event. We calculate quantum-mechanically the probability of hopping to a neighbor interstice for an atom which simultaneously interacts with the electron system in the nonequilibrium current state, thus taking into account self-consistently the nonadiabaticity effects in electromigration. As a result, a general expression for net atomic current is obtained which includes both diffusion and conduction contributions, and in the linear response approximation obeys the Nernst-Einstein relation between mobility and diffusion coefficient. The driving force for electromigration is found to consist of a direct term and a wind force. The latter differs substantially from the appropriate results of adiabatic theories, and coincides with the Fiks-Huntington momentum-transfer expression^{8,9} only in the limit $k_F d \ll 1$, where k_F is the electron Fermi momentum and d is the hopping distance. In the general case, we find that the wind force includes a phase factor reflecting the effect of the change in the atom's position during the electron-atom scattering event. This results in a substantial decrease of the wind force for $k_F d \geq 1$, due to the recoil effects associated with electron momentum transfer to the lattice because of strong atom-phonon polaron coupling.

For the sake of simplicity we have restricted ourselves to the limit of weak atom-electron scattering treated within the Born approximation, and we assume a significantly strong phonon-polaron effect. This makes it possible to neglect the electron-polaron reduction of the atom diffusion coefficient. We also neglect the screening of the external electric field by electrons, which formally corresponds to the limit of small "bare" valence of the impurity ion¹⁵ and is consistent with the assumption of weak atom-electron interaction.

Our result for the electromigration drift velocity \vec{u} for the impurity atoms turns out to have precisely the Nernst-Einstein form, namely,

$$\vec{u} = \frac{D}{k_B T} \vec{F}_{net},$$

where D is the diffusion coefficient, k_B is Boltzmann's constant, and T is the temperature. The quantity \vec{F}_{net} may be regarded as a net driving force here, and our detailed derivation gives the following pleasing form for this quantity:¹⁶

$$\vec{F}_{net} = \vec{F}_d + \vec{F}_w,$$

where \vec{F}_d is the usual direct-force contribution ($\vec{F}_d = Ze\vec{E}$), and the electron-wind contribution \vec{F}_w to the net driving force \vec{F}_{net} is determined by the expression:

$$\vec{F}_w = \frac{4\pi}{d} \sum_{\vec{k}\vec{k}'} |V_{00}(\vec{k}, \vec{k}')|^2 \sin[(\vec{k} - \vec{k}') \cdot \vec{d}] f_{\vec{k}}(1 - f_{\vec{k}'}) \delta(\epsilon_{\vec{k}} - \epsilon_{\vec{k}'}),$$

where \vec{d} is the jump-vector from initial to final sites, $V_{00}(\vec{k}, \vec{k}')$ is the electron-atom scattering potential matrix-element, and $f_{\vec{k}}$ is the electron distribution function for an electron in state \vec{k} and energy $\epsilon_{\vec{k}}$. In the limit of small electron Fermi-momentum, this formula for \vec{F}_w turns out to be exactly the same as the momentum-transfer expression of the ballistic model^{8,9} for a fixed impurity in the ground state. The latter expression, for the system considered here is

$$\vec{F}_w^{ballistic} = 4\pi \sum_{\vec{k}\vec{k}'} |V_{00}(\vec{k}, \vec{k}')|^2 (\vec{k} - \vec{k}') f_{\vec{k}}(1 - f_{\vec{k}'}) \delta(\epsilon_{\vec{k}} - \epsilon_{\vec{k}'}).$$

Our expression for the electromigration drift velocity \vec{u} represents an important result in electromigration theory in that it is the result of a self-consistent treatment in which the interacting atom-electron-phonon system is treated simultaneously.

The effective wind force \vec{F}_w in our theory turns out to be related to the corresponding wind force $\vec{F}_w^{ballistic}$ in the Fiks-Huntington^{8,9} ballistic model by a rather simple analytic expression, which depends only on the hopping distance d and the Fermi wavevector k_F . The result which we have found is¹⁶

$$\vec{F}_w = \alpha \vec{F}_w^{ballistic},$$

where

$$\alpha = -\frac{3}{2x^3} \left(\sin 2x + \frac{\cos 2x - 1}{x} \right),$$

and we have defined $x = k_F d$. The function $\alpha(x)$ has the property that it rapidly falls from the value unity at $x = 0$ to the value zero at $x = \pi$. Because of this functional dependence of α on the parameter $x = k_F d$, one can expect a substantial reduction of electron-wind force for light interstitial impurities in metals. This behavior is due to the

strong recoil effect for electron scattering by the hopping atom-polaron. In the case of hydrogen diffusion in metals for which our approach should be most appropriate, typical estimated values of x are between 2 and 4 (~ 1.8 for hopping between tetrahedral interstices in bcc Nb, and $\sim 3.7 - 3.8$ for octahedral sites in fcc Pd and Cu³⁵). Therefore, a proper analysis of experimental data on electromigration in such systems requires the use of our general nonadiabatic expression for the wind force rather than the ballistic expressions.

We have succeeded in generalizing the quantum mechanical analysis described above to take into account non-adiabaticity in the electron-screening response as well as in the wind force. This allows us to investigate the non-adiabatic corrections to the direct force as well as the wind force. (The direct force is very sensitive to the electron screening in the vicinity of the defect.) We have considered the realistic situation of multi-level impurity states in individual interstitial potential wells. It turns out that for low enough temperatures, namely, $k_B T \ll \hbar\omega$, where $\hbar\omega$ is the energy gap between intra-well impurity levels, and for weak impurity electron interaction, atomic transport occurs via ground-level impurity hopping. In this regime, electromigration is associated with the hopping probability involving anti-adiabatic electronic response to the change in the equilibrium impurity position upon completion of a successful jump.

We have carried through the analysis of the electromigration driving force, using methods similar to those we used earlier¹⁶. We explicitly obtain electron-wind and direct-force contributions to the net atomic current, and we find that the electromigration contribution to the macroscopic atomic current obeys the Nernst-Einstein relation between atomic current and an effective driving force. The only trace of impurity dynamics in the effective driving force is the specific combination of local electron density and interaction potential that appears in the final expression for the effective driving force. This combination reflects the fact that both interstices (initial and final) are equally shared by the tunneling impurity atom at the moment of a successful jump. The effect is purely anti-adiabatic and shows itself in the renormalization of both the electron wind force and the screening correction to a direct force as compared to the results of adiabatic theory.¹¹ This renormalization, which is determined by an interference phase-factor, is in general more pronounced for the wind force contribution associated with the real processes of elastic scattering of electrons at the Fermi surface. On the other hand, the dynamical screening of the direct force due to the local electron pile-up involves electrons from the whole Fermi sea, which smears out the interference effect.

We find that our general formula for the electromigration driving force gives a wind-force contribution identical to that which we presented earlier in this Section.³⁶ The direct-force contribution is the new feature in our latest work, and we have been able to derive

an analytic expression for this contribution. Our expression is similar to that obtained in the usual adiabatic picture¹¹ except for the presence of a renormalization factor $\gamma(x) = 3(\sin x - x \cos x)/x^3$ in the integrand of the integral expression for the direct valence Z_d , where the integration is over all x , and $x = k_F d$ is the product of the Fermi wavevector k_F and the jump distance d . This renormalization can result in an enhancement or a reduction of Z_d depending on the actual value of the parameter $k_F d$. The magnitude of the renormalization can be on the order of 20% or more of the bare valence Z in typical cases. Our self-consistent microscopic derivation of the general expression for a direct impurity valence helps resolve the “direct force controversy” between the results of different adiabatic approaches to the screening effects in electromigration.

VII. NUMERICAL SIMULATIONS AND DYNAMICAL EFFECTS IN ELECTROMIGRATION

In order to explore further such dynamical effects as local heating and recoil enhanced atomic migration, we have performed numerical simulations of electromigration. We considered the classical motion of an impurity in a periodic potential due to the crystal. The impurity is subjected to a series of random thermal impulses from a bath at thermal equilibrium, while the wind force is simulated by a random sequence of impulses in the direction of the electron wind. This study is an attempt to obtain a verification of our non-adiabatic, recoil-enhanced atomic-migration mechanism,³⁷ and to examine the effects of local heating in the atomic motion.

In the standard adiabatic picture, the electromigration driving force is calculated as if the impurity were infinitely massive and atomic recoil effects are neglected. In this picture, the force so determined is then to be used as a static perturbation which tilts the atomic potential and causes an atomic current. In reality, the electron-wind force is a series of impulses due to individual electron collisions, and the atom will generally recoil and absorb energy in these collisions. For classical diffusion mechanisms, it is the energy transfer that is responsible for electromigration. But energy transfer depends on the velocity of the atom at the time of collision, the transfer being larger when the atom is moving at a larger velocity. This in turn leads to an atomic current that is enhanced over the value calculated in the purely adiabatic picture. This enhancement is expected to be a significant effect for the case of light interstitial impurities such as hydrogen, especially in mesoscopic systems, where the off-equilibrium electron distribution can contain a substantial “hot electron” component that is virtually unaffected by Pauli-exclusion principal restrictions on the allowed energy transfer per collision. To clarify the role of dynamical effects in

electromigration , we have devised a simple model, which allowed us to perform the first numerical simulations of the electromigration process at the atomic level.

Our model is appropriate to the the classical diffusion regime, where an atom jumps over a potential barrier between two equivalent sites. We take the atom to be located in a periodic potential, $U(X)$, having the following sinusoidal form

$$U(X) = \frac{1}{2}E^* [1 - \cos(2\pi x/d)],$$

where E^* is the height of the potential barrier and d is the jump distance (the periodicity length). The atom is subjected to thermal collisions at an average frequency ν_{th} , and these collisions randomize the atom velocity towards the equilibrium Boltzmann distribution. In addition, the atom is subjected to collisions with the off-equilibrium electrons, at an average frequency ν_{el} , which is proportional to the product of electron current and the scattering cross-section. (We estimate $\nu_{el} \sim 10^9 s^{-1}$ when $J \sim 10^6 A/cm^2$ and the scattering cross-section $\sigma \sim 1 \text{ \AA}^2$.) All collisions are taken to occur randomly via a Poisson process, i.e., there is an exponential distribution of waiting times for thermal collisions and for electron collisions. For simplicity, we can assume a constant momentum transfer, p , for each electron collision. The waiting times are easily obtained with the aid of a random-number generator algorithm. The motion of the atom between collisions is calculated by means of a fourth-order Runge-Kutta algorithm.³⁸ At the moment of a thermal collision, as found by the random-number generator, the atom takes on a new velocity determined by random sampling of the Boltzmann velocity-distribution. At the moment of a collision with an impulse due to the electron-wind, also with occurrence times determined by the random-number generator, the atom's velocity is increased in the electron-wind direction by p/M , where M is the atom's mass.

The model that we have devised contains an interesting scaling feature with respect to mass M . If we measure all times in terms of the period of oscillation t_o for the atom when it is at the bottom of its potential well, where the motion is harmonic, then the atom current J appropriate to the case where the momentum transfer is p (and for fixed values of E^* , ν_{th} , and ν_{el}) satisfies the scaling relation $J(p', M') = J(p, M)$ provided that $p' = p/\sqrt{M'/M}$. Thus, for example, the plot of J vs. p for an aluminum atom is the same for J vs. p for a hydrogen atom provided that for aluminum we use values of p that are $\approx 1/\sqrt{27} = 0.192$ times the value that would be used in the plot for hydrogen (assuming that the other parameters are fixed as stated).

Although our model is relatively simple, the computer calculations are difficult because the rarity of an atomic jump requires the computations to extend over a huge number of

time steps. The situation is more tractable for smaller activation energies E^* , but even so, a very large number of time steps is required to obtain good enough numerical data for meaningful statistics. To make the computations manageable, we have chosen a relatively small activation energy ($E^* = 0.2eV$). We find that the net atom flux in the direction of the electron wind does have the expected linear variation with the collision frequency ν_{el} for collisions between the off-equilibrium electrons and the diffusing atom. We have verified that the net atom flux is linear in ν_{el} for all physical values of ν_{el} . This implies that the electromigration current of atoms is linear in the electronic current density. Because of this, we can crank-up the strength of ν_{el} (or the electron current density) and obtain meaningful results, i.e., we need not use the extremely small electron drift velocity that one typically has in the experimental situation, but instead we can use much larger values for the incident electron current. This in turn makes our computations less costly, since there is less noise in the computer output when the electron current density is larger. Even so, we required on the order of a billion time steps to amass meaningful statistics for the atom current J at a single value of p , with all other parameters fixed. Although the net atom current is linear in ν_{el} , and hence linear in the electron current, the same is not true for the dependence of the net atom current on the momentum transfer p per collision. In fact, our main concern is with studying the recoil-enhancement effect, and this shows up as a non-linearity in the J vs. p curve.

Calculations have been performed for the case of hydrogen atoms. The results for the net atomic current are presented in Fig. 9 for the case that $\nu_{th}t_o = 5.0$ and $\nu_{el}t_o = 0.1$. The distance d is chosen to be 2.75\AA . The period t_o is defined to be $\sqrt{K/M}$, where $K^2 = 2\pi^2E^*/d^2$ is the effective spring constant at the bottom of a well. It is convenient to express the atom current in terms of the net number of jumps per time period t_o made by an atom in the direction of the electron wind. We call this the net atom flux, and it is the quantity shown in Fig. 9 as a function of the momentum transfer per collision. The values of momentum p are given in the computational units $\sqrt{\text{amu} \times \text{eV}} = 1.60 \times 10^{-23}$ kg m/s. Each point corresponds to a run containing on the order of 100,000 total jumps (leftward plus rightward jumps), but the net number of jumps to the right (rightward minus leftward) is a small fraction of the total. Evaluation of each point in Fig. 9 took about 8 hours of computer time on a Sparcstation ELC.

The results in Fig. 9 indicate a significant enhancement effect for hydrogen. This effect is manifested by a non-linearity in the atom current as a function of momentum transfer p . In the adiabatic model the wind-force equals $\nu_{el}p$, which is the time average force.³⁷ Departures from this linear behavior with respect to p indicate an enhancement. In particular for $p \approx 0.23$ computational units, which corresponds to electron momentum

transfers for backscattering on the Fermi surface of aluminum metal, we see that the atomic current for hydrogen electromigration is on the order of five times as large as would be obtained from a linear curve extrapolated from small p values. The corresponding enhancement for aluminum is much smaller, however. According to our scaling relation, the enhancement for an aluminum atom would be only on the order of a few percent. These results show that our theoretical ideas³⁷ concerning recoil-enhanced atomic migration are valid.

It is possible to push these calculations to higher activation energies, but the time required for a run will quickly become prohibitive. However, if the temperature is raised as larger values of E^* are chosen, the run-time can be kept reasonable. For example, the J vs. p calculation for $E^* = 0.4$ eV and $T = 600$ K takes about the same time to run as does the curve shown in Fig. 9. It turns out that the results are quite similar—the curve has about the same shape as in Fig. 9, but the values of atom flux are on the order of one-half as large as in Fig. 9. A factor of one-half would be expected on the basis of a Nernst-Einstein relation giving $J \propto D/T$, and a simple diffusion model giving $D \propto t_o^{-1} \exp(-E^*/k_B T)$. It would then follow that the atom current measured in the number of jumps in time t_o would be inversely proportional to T .

We have recently pushed the numerical simulations to the case where $E^* = 0.3$ eV and $T = 300$ K. This requires about an order of magnitude more run-time than for the two cases discussed above. The results for hydrogen are shown in Fig. 10. (The values of $\nu_{th} t_o$ and $\nu_{el} t_o$ are the same as for Fig. 9.) Each point required about four days of run-time on a Sparcstation ELC. The results show an extremely large enhancement factor setting-in for values of p beyond 0.10. According to our theoretical estimates of the recoil enhancement effect³⁷, the net atom flux is expected to behave roughly as $(k_B T/v^* p) \sinh(v^* p/k_B T)$, where $v^* = \sqrt{2ME^*}$. This is consistent with the very large enhancement at larger p in the case of larger E^* values. It should be cautioned, however, that such large enhancements in metallic systems are only likely to occur in mesoscopic rather than bulk systems because collisions in which the electrons transfer a very large amount of energy relative to $k_B T$ are blocked by the Pauli-exclusion principle in a bulk metal. In a mesoscopic system, as mentioned earlier, relatively large perturbations in the incident electron distribution are possible, and this makes Pauli-blocking inoperative.

It is interesting that the classical diffusion model considered here gives an enhancement of the effective wind force, whereas the quantum-mechanical theory gives a de-enhancement factor (the quantity α in Section VI). This is not an inconsistency, but is in fact in agreement with theoretical ideas we have put forward.³⁷ The point to consider is that quantum diffusion processes and classical diffusion processes are very different, and occur

in very different regimes. In the classical case, one expects that the energy transfer is the important thing in helping an atom go over a barrier, and this energy transfer is more efficient when the atom is moving in the direction of the impulse. On the other hand, in a quantum hop, the electron scattering tends to de-tune the below-barrier tunneling process, and so the opposite effect occurs.

The calculations described here represent the first computer simulations of electromigration at the atomic level. Although the model is rather oversimplified, it does reveal interesting dynamical effects which transcend the conventional adiabatic picture. Clearly, computer simulations of electromigration are an interesting area for future studies.

VIII. ELECTROMIGRATION-INDUCED FAILURE AND MTF FOR METALLIZATIONS

In our previous work we analyzed the microscopic driving forces for electromigration. This force is proportional to the local transport electric field, and all information about the microscopic transport mechanism is contained in the appropriate coefficient Z^* , which is the effective charge of the atomic defect. Assuming that Z^* is known, we are in a position to address a critical problem in applied electromigration work, namely, irreversible damage to thin film metallization in integrated circuits.

Because of the driving force, in general there will be a net divergence of atomic flux at inhomogeneities in the microstructure. This leads to mass depletion (accumulation) and formation of voids (extrusions). The actual failures occur when the growing voids coalesce to form an open circuit in the current passage (or extrusions result in short circuits between different conducting lines). In order to prevent extrusion-related failures, a passivation (usually glassy) layer is put on the metallization, thereby eliminating surface diffusion. Electromigration-induced failures then occur as a result of void formation at those points in the grain boundary network where outgoing atomic flux exceeds the incoming flux. Such void nucleation centers (most commonly, triple points where three or more grains join together) are randomly distributed in the metallization, with the average separation distance being on the order of the typical grain size.

The major reliability issue for microelectronic devices is the estimation of the mean time to failure (MTF) and finding ways to increase it. The only practical way to estimate MTF experimentally is to perform an accelerated failure test at high enough electric current density j and temperature T and extrapolate the obtained data to real-life operating conditions using a particular relation $MTF = MTF(j, T)$ based upon some theoretical model.

A number of models have been used to predict the dependence of electromigration failure times for thin metal films on electric current density and temperature. These models differ substantially on whether the actual lifetimes are controlled mainly by void incubation or their subsequent growth and on how important the local Joule heating is. However, almost invariably, these models have one important thing in common, namely, it is assumed that electromigration damage occurs exclusively via grain boundary diffusion and the primary failure mechanism is the same for both use and test conditions. A useful Arrhenius-like relation was first formulated empirically by Black³⁹ to extrapolate test data to real-life operating conditions. The much-used Black equation for the MTF is

$$MTF = Aj^{-n}e^{-E/k_B T},$$

where A is a material constant and E is the activation energy for electromigration-induced failure. It was pointed out by a number of authors⁴⁰⁻⁴² that actual failure mechanisms and, consequently, the resulting function $MTF(j, T)$ (e.g., the value of n in Black's equation) under high current stress and at elevated temperatures appropriate for test conditions can be quite different from those corresponding to real-life operating conditions. For example, if local Joule heating is inessential and the failure occurs by void growth at sites of abrupt changes in atomic flux, then $n = 1$. At high enough currents, when the failure is substantially accelerated by a local temperature increase due to the current crowding effect in the immediate vicinity of a growing void, larger values $n \geq 2$ should be observed. The value $n = 2$ is also characteristic of the regime of incubation-controlled electromigration failure in the absence of local heating effects.^{43,44} Experimentally, it has been found that $n \simeq 2$ in aluminum under typical test conditions ($j \simeq 1 - 2 \times 10^6$ A/cm², $T \simeq 150^\circ\text{C}$). But since the failure mechanism can change at low current densities, which may result in the value $n = 1$ in that regime, the legitimacy of the extrapolation to the operating conditions made with $n = 2$ is questionable.

Another, even more important, issue here is whether the activation energy E for electromigration failure in Black's equation has the same value under test and operating conditions. In all theoretical models that one finds in the literature and, consequently, in extrapolation results based upon them, the assumption is made that E is nearly constant within the whole range of relevant values of the temperature and current density. This assumption rests on the idea that only grain boundary atomic diffusion is essential for

electromigration-induced failure in both test and real-life operating situations. This idea seems to be a natural consequence of the relation

$$\frac{J_l}{J_b} \sim \frac{d}{\delta} \cdot \frac{D_l}{D_b},$$

where J_l, J_b are atomic fluxes due to electromigration in the lattice and at the grain boundaries respectively, D_l, D_b are corresponding diffusivities, d is the typical grain size, and δ is the effective grain boundary width. (For simplicity, atomic densities and effective charges in the lattice and at the grain boundaries are assumed the same.) For a thin metal film with a micron grain size at $T \lesssim 0.5 T_m$, where T_m is the melting point, one obtains the estimate $J_l \ll J_b$, which is considered a sufficient justification for the complete neglect of lattice diffusion.

At the same time, it is obvious that in the situation of a completely passivated metallization electrically connecting two semiconductor elements, and with atomic flux blocked at the metal-semiconductor contact surfaces, no major electromigration damage can occur without lattice diffusion. Indeed, with the whole surface of the metal strip (including its blocked ends) unavailable for atomic transport the only way for nucleating voids to grow is that the removed matter spreads out either into the grain boundaries or into the lattice or causes the passivation to lift and/or crack (delaminations/extrusions). If the void nucleation centers are distributed randomly but on the average uniformly throughout the film with the separation distance l , then in the absence of lattice diffusion the typical ultimate void size is $\sim (c_0 l \delta)^{1/2}$, where $c_0 < 1$ is the equilibrium grain boundary vacancy concentration per atom. Since $l \gtrsim d \gg \delta$, this maximum size is much smaller than l , and it is very unlikely that such small voids can somehow coalesce and form an open circuit in the film. In other words, large scale damage with the net fractional volume of the voids much larger than $c_0 \delta / l$ can only occur if the removed matter spreads out into the lattice. Therefore, when considering advanced stages of electromigration damage and actual failures in metallizations with blocked surface diffusion one has to take into account the atomic flux from the grain boundaries into the lattice. The failure rate, which is proportional to the rate of void growth, is then proportional to the density of this flux.

The most important question that now arises is whether the intensity of this electromigration-induced flux is determined by grain boundary or lattice diffusion. The answer depends on the relation between the length l of a grain boundary segment connecting two neighboring voids and the diffusion length $(D_b \tau)^{1/2}$ of a nonequilibrium atom (vacancy), associated with its lifetime τ in the grain boundary.

In the situation when $(D_b\tau)^{1/2} \ll l$, all the atoms "injected" into the grain-boundary segment from the growing void and driven along by electromigration readily escape into the lattice by the time they would have reached the opposite end of the segment. Hence, there are no restrictions on the electromigration atomic flux (vacancy flux "feeding" the void) associated with the escape process, and the intensity of this flux is determined only by the grain boundary diffusivity D_b . The resulting expression for the vacancy flux feeding the growing void, $J_0 \simeq n_0 D_b F / k_B T$ (n_0 is the equilibrium vacancy density, F is electromigration driving force), is the same as the one used by all existing models based upon the assumption of vanishingly small lattice diffusion and an infinite grain boundary. In the absence of local heating effects, this corresponds to the activation energy E for failure in Black's equation being equal to E_b , the activation energy for grain boundary diffusion.

In the opposite limiting case $(D_b\tau)^{1/2} \gg l$ atoms leaving the void are not able to escape from the grain boundary segment by the time they reach its end, which results in a bottleneck effect causing a drastic decrease in the electromigration flux. An MTF analysis in this regime is outlined below.

It should be emphasized that our approach is appropriate only if the passivation layer remains unchanged and perfectly adheres to the metallization surface during void growth. Under high enough atomic flux stress, which is typical for most test conditions due to large current densities, the passivation is likely to lift and/or crack at certain weak spots. As a result, the matter removed in the course of void growth is spread out in the form of extrusions and the failure rate can increase dramatically. However, here we restrict our analysis to normal operating conditions, i.e., relatively low current densities, and assume that the passivation remains perfectly undamaged until, perhaps, the last stage of electromigration-induced failure.

Consider a simple 1-d model of a single grain boundary consisting of alternate segments with higher (D_+) and lower (D_-) diffusivities. If we choose the x -axis along the grain boundary in the direction of the electromigration vacancy flux (opposite to actual atomic flux), then the points x_n of abrupt negative change in the diffusivity, such that $D(x_n - 0) = D_+$ and $D(x_n + 0) = D_-$, are the nucleation centers for accumulation of vacancies and subsequent void growth. These points correspond to grain boundary junctions where the incoming electromigration vacancy flux exceeds the outgoing flux. Similarly, the points of abrupt positive change in the diffusivity (from D_- to D_+), which are the vacancy depletion centers, correspond to the junctions where the outgoing vacancy flux exceeds the incoming one.

The transport equation for vacancies in any particular grain boundary segment has the form

$$\frac{\partial n}{\partial t} + \frac{\partial J}{\partial x} = \frac{n_0 - n}{\tau},$$

where n is local vacancy density, n_0 is its equilibrium value, and τ is the vacancy lifetime in the grain boundary. J , the x -component of the vacancy flux, is given by

$$J = D_b \left(\frac{F}{k_B T} n - \frac{\partial n}{\partial x} \right).$$

Here D_b is the appropriate diffusivity, and the driving force F for vacancy electromigration can be written in the standard form

$$F = -Z^* e \rho j,$$

where Z^* is the effective atomic valence for electromigration, ρ is the resistivity of the film, and j is the x -component of dc electron charge-density current. In writing the vacancy-flux equation (with $T = \text{const}$), we have taken into account only the electromigration and diffusion components of vacancy flux, thus neglecting all contributions associated with local heating effects and temperature gradients. According to existing estimates (see, for example, Ref. 45), this is a very good approximation for typical operating conditions ($j < 5 \times 10^5$ A/cm²). We will also neglect for simplicity all local changes in electron current density j due to the changing cross-sectional area of the film and current crowding associated with continuous void growth, which is appropriate for early enough stages of electromigration damage.

Following most authors, we assume that the vacancy dynamics occur in two distinct phases: First, void incubation, and, second, actual growth. During the incubation phase, vacancies keep accumulating at the nucleation centers until their supersaturation level $S = (n - n_0)/n_0$ reaches some critical value \bar{S} . As soon as this critical supersaturation has been reached, the accumulated vacancies coalesce instantaneously thus nucleating macroscopic voids. At this point the second phase begins and the voids start growing continuously, with the supersaturation sustained at the level \bar{S} , until an open circuit failure occurs. An important issue here is that the value of \bar{S} in a passivated metal film is substantially reduced by the presence of tensile mechanical stress and can be as small as ~ 0.01 .^{44,46} Therefore, the incubation time is short, and with the void growth slowed down drastically by the earlier discussed bottleneck effect at low enough temperatures and current densities, the actual failure times under operating conditions should be completely growth-controlled.

To proceed further we invoke a simple model in which we consider voids growing uniformly (on average) along 1-dimensional segments. We find that the crucial length parameters in the analysis are the following: The distance l between nucleation centers, the grain-boundary diffusion-length L_τ defined by $L_\tau = (D_b\tau)^{1/2}$, and the electromigration length L_F , defined by $L_F = |k_B T / Z^* e \rho j|$. The two regimes of interest are

$$L_F, L_\tau \gg l \quad \text{Bottleneck}$$

$$l, L_\tau \geq L_F \quad \text{No bottleneck.}$$

Estimates from normal operating conditions (non-test situations) in aluminum, give $L_F \sim 40\mu\text{m}$, $L_\tau \sim 30\mu\text{m}$, and $l \sim 1\mu\text{m}$ for $Z^* = -10$ and $j = 3 \times 10^5 \text{ A/cm}^2$ at room temperature. This puts us in the bottleneck regime. On the other hand, if we have much higher currents and somewhat higher temperatures then it is possible to be in the no-bottleneck regime. Most important, it is possible to make this transition from one regime to the other simply by going from moderately high electron current density to very high electron current density. Thus, there would be different observed values of the activation energy E for field conditions and accelerated test conditions.

The result of our analysis⁴⁷ is that in the no-bottleneck regime, the atom (or vacancy) current density has the usual Nernst-Einstein form

$$J_0 = n_0 D_b F / k_B T,$$

while in the bottleneck regime, the atom (or vacancy) current is

$$J \sim n_0 l^2 \tau^{-1} F / k_B T.$$

Thus, the ratio of atom (or vacancy) currents is

$$J/J_0 \sim l^2 / D_b \tau,$$

and with MTF being inversely proportional to current, we obtain

$$\frac{MTF}{MTF_0} \sim \frac{D_b \tau}{l^2},$$

or

$$\frac{MTF}{MTF_0} \sim \frac{a\delta}{l^2} e^{-(E_l - E_b)/k_B T}.$$

Estimates for aluminum at 300K with $a = 2\text{\AA}$, $\delta = 5\text{\AA}$, and $l = .1\mu\text{m} - 1\mu\text{m}$ give $MTF/MTF_0 \sim 10^3 - 10^5$ for the ratio by which the MTF is enhanced by the bottleneck effect.

The analysis we have described represents a first attempt to self-consistently analyze electromigration-induced failures in passivated metallizations. The important issue of possible damage caused to a passivation layer by persistent atomic flux is not addressed here. In our analysis, we assumed that this damage can occur only when atomic flux exceeds a certain critical value that is sufficiently large for a high-quality passivation. Therefore, as long as actual electromigration-induced atomic flux, which is drastically reduced by the bottleneck effect at low operating temperatures, remains smaller than this critical value, the results obtained in the present paper should be applicable. The estimation of this critical atomic flux and the construction of a self-consistent description of electromigration-induced failures in the presence of broken passivation is a complicated problem which requires further analysis.

IX. CONCLUSION

Our investigation of microforces in electromigration has led to a better understanding of the electromigration phenomenon on several levels. At the microscopic level, we find that in the immediate vicinity of a defect complex, a local transport field is set-up, and this field acts as the driving force for electromigration. The electron-wind part of the local field correlates with the residual resistivity of the complex, as was shown in Sec. II for the case of an impurity near a grain boundary or dislocation. This correlation implies a connection between electromigration and $1/f$ -noise due to impurity motion. The local field can be probed with an STM and this provides a link between electromigration and STM measurements, as shown in Sec. III. The mesoscopic system consisting of the STM tip and an impurity at or near a surface defines a mesoscopic system whose I - V characteristics give information about electromigration driving forces. A related mesoscopic system, namely the "point-contact," can, in fact, be used to measure the direct force in electromigration, and this is shown in Sec. IV. The underlying phenomena that makes this measurement possible is the electron-current concentration and breakdown of the local form of Ohm's Law ($\vec{j} = \sigma \vec{E}$) in the immediate vicinity of the point-contact.

The relationship between inelastic scattering, electronic conductivity, and local heating is an important one, and is investigated in detail for a mesoscopic system in Sec. V. Because electrons transfer energy to an impurity (or some other atom in a defect complex), the electronic conductivity will show definite non-linear structure in the I - V curves. From the point of view of the target atom, the energy deposited by the off-equilibrium electrons

provides local heating at the microscopic level. This local heating can have a profound effect on electromigration, as it may provide the otherwise scarce energy for the atom to complete a diffusion jump. This enhancement of electromigration due to recoil energy deposition to a target atom occurs for classical over-the-barrier atomic jumps. In the quantum tunneling regime, however, the situation is different. As shown in Sec. VI, the recoil effect tends to degrade the efficiency of atomic tunneling, and electromigration is diminished.

Further studies of dynamical effects in electromigration were undertaken by means of numerical simulations. These simulations, which are described in Sec. VII, are the first for electromigration at the atomic level. Our results indicate that large enhancement effects are possible, especially for light impurities in mesoscopic systems. We also addressed the more practical problem of electromigration-induced failure in metallizations. The analysis described in Sec. VIII represents the first attempt to analyze self-consistently the failure time in ideally passivated metallizations. We find that a bottleneck situation exists in which failure-times are governed by the lattice diffusion rather than grain-boundary diffusion. This results in a much longer time to failure than would be expected from usual models.

Finally, we point out that as electronic devices become progressively smaller and begin to function exclusively in the mesoscopic domain, the phenomena which we have investigated in this work will take on increasing importance. Specifically, local fields, resistivity fluctuations, current concentration, local heating, and quantum diffusion processes will be central to the operation of next-generation devices. A better understanding of these phenomena is needed to assure the proper functioning of the mesoscopic and nano-scale devices of the future. The work described in this report represents a first step in that direction.

REFERENCES

1. R.S. Sorbello, Technical Report RADC TR-90-15, March 1990 (Rome Air Development Center, Griffiss Air Force Base, NY).
2. C.S. Chu and R.S. Sorbello, Phys. Rev. B **38**, 7260 (1988).
3. C.S. Chu and R.S. Sorbello, Phys. Rev. B **40**, 5950 (1989).
4. R.S. Sorbello, Phys. Rev. B **39**, 4984 (1989).
5. R. Landauer, IBM J. Res. Develop. **1**, 223 (1957).
6. N.W. Zimmerman and W.W. Webb, Phys. Rev. Lett. **61**, 889 (1988); J. Pelz and J. Clarke, Phys. Rev. B **36**, 4479 (1987).
7. C.S. Chu and R.S. Sorbello, Phys. Rev. B **42**, 4928 (1990).
8. V.B. Fiks, Fiz. Tverd. Tela (Leningrad) **1**, 16 (1959) [Sov. Phys. Solid State **1**, 14 (1959)].
9. H.B. Huntington and A.R. Grone, J. Phys. Chem. Solids **20**, 76 (1961).
10. L.J. Sham, Phys. Rev. B **12**, 3142 (1975).
11. R.S. Sorbello and B. Dasgupta, Phys. Rev. B **16**, 5193 (1977).
12. W.L. Schaich, Phys. Rev. B **19**, 620 (1979).
13. R. Landauer, Phys. Rev. B **14**, 1474 (1976).
14. P.R. Rimbey and R.S. Sorbello, Phys. Rev. B **21**, 2150 (1980).
15. R.S. Sorbello, Phys. Rev. B **31**, 798 (1985).
16. I.F. Itskovich and R.S. Sorbello, Phys. Rev. B **45**, 718 (1992).
17. C. Bosvieux and J. Friedel, J. Phys. Chem. Solids **23**, 123 (1962).
18. L. Turban, P. Nozieres and M. Gerl, J. de Phys. **37**, 159 (1976). (1980).
19. A.H. Verbruggen, IBM J. Res. Dev. **32**, 93 (1988).
20. Yu. V. Sharvin, Zh. Eksp. Teor. Fiz. **48**, 984 (1965) [Sov. Phys.-JETP **21**, 655 (1965)].
21. I.K. Yanson, Zh. Eksp. Teor. Fiz. **66**, 1035 (1974) [Sov. Phys.-JETP **39**, 506 (1974)].
22. I.O. Kulik, A.N. Omel'yanchuk, and R.I. Shekhter, Fiz. Nizk. Temp. **3**, 1543 (1977) [Sov. J. Low Temp. Phys. **3**, 740 (1977)].
23. I.F. Itskovich and R.S. Sorbello, Solid State Commun. **82**, 729 (1992).
24. I.K. Yanson, Fiz. Nizk. Temp. **9**, 676 (1983) [Sov. J. Low Temp. Phys. **9**, 343 (1983)].
25. R. Landauer, Phil. Mag. **21**, 863 (1970).
26. M. Büttiker, IBM J. Res. Dev. **32**, 317 (1988).
27. Z. Chen and R.S. Sorbello, Phys. Rev. B **44**, 12857 (1991).
28. S.W. Lovesey, *Condensed Matter Physics: Dynamical Correlations* (Benjamin Cummings Publishing Co., New York, 1986).
29. C.S. Chu and R.S. Sorbello, Phys. Rev. B **40**, 5941 (1989).
30. K. S. Ralls, D. C. Ralph and R. A. Buhrman, Phys. Rev. B **40**, 11561 (1989).

31. Z. Chen and R.S. Sorbello, "Local Heating in Mesoscopic Systems," submitted to Phys. Rev. B.
32. C.P. Flynn and A.M. Stoneham, Phys. Rev. B **1**, 3966 (1970).
33. Yu. Kagan and M.I. Klinger, J. Phys. C **7**, 2791 (1974).
34. Yu. Kagan and N.V. Prokof'ev, Sov. Phys. JETP **63**, 1276 (1986).
35. Numerical values for these transition metals are just rough estimates obtained by using k_F values which correspond to appropriate Fermi energies in band-structure calculations. See, for example, Reference 15.
36. I.F. Itskovich and R.S. Sorbello, "Quantum Theory of Electron Screening and Non-adiabaticity Effects in Electromigration," submitted to Phys. Rev. B.
37. R. S. Sorbello, Phys. Rev. Lett. **63**, 1815 (1989).
38. W.H. Press *et al.*, *Numerical Recipes: The Art of Scientific Computing* (Cambridge University Press, 1985).
39. J. R. Black, IEEE Trans. Electron Devices **ED-16**, 338 (1969).
40. I. A. Blech, Thin Solid Films **13**, 117 (1972).
41. F. M. d'Heurle & P. S. Ho, *Electromigration in Thin Films* (IBM Research Report, Yorktown Heights, New York, 1977).
42. R. A. Sigsbee, J. Appl. Phys. **44**, 2533 (1973).
43. M. Shatzkes & J. R. Lloyd, J. Appl. Phys. **59**, 3890 (1986).
44. J. R. Lloyd, J. Appl. Phys. **69**, 7601 (1991).
45. Y.S. Chaug and H.L. Huang, J. Appl. Phys. **47**, 1775 (1976).
46. J. R. Lloyd, in *Materials Reliability Issues in Microelectronics*, edited by J.R. Lloyd, F.G. Yost and P.S. Ho (Materials Research Society Symposium Proceedings Series, Vol. 225) pp. 47-52.

FIGURE CAPTIONS

- Figure 1. Relative change in resistivity for an impurity near a grain boundary of thickness D in an aluminum film. Curves are shown for the cases that $D = 2$ a.u., 4 a.u. and 8 a.u. (1 a.u. = 0.53 Å). The grain boundary lies in the region $-D/2 \leq z \leq D/2$, and the electron wind is in the z -direction (perpendicular to the grain boundary). Results are shown for the case that the impurity is described by an s-wave phase shift, with the value of the phase shift, δ_o , set equal to the ratio of grain boundary potential strength, U , over the Fermi energy, E_F . (The results scale linearly with the quantity $(U/E_F)/\delta_o$.) The relative change in the electromigration wind force on an impurity is equal to one-half of the relative change in resistivity for this model.
- Figure 2. Relative change in resistivity for an impurity near a dislocation of radius equal to 2 a.u. in an aluminum film. The dislocation lies in the region $0 \leq R \leq 2$ a.u., and the electron wind is perpendicular to the axis of the dislocation. The impurity is at a distance R from the center of the dislocation and at an azimuthal angle ϕ with respect to the direction of the electron wind. Three cases for ϕ are shown. Results are shown for the case that the impurity is described by an s-wave phase shift, with the value of the phase shift, δ_o , set equal to the ratio of dislocation-core potential strength, U , over the Fermi energy, E_F . (The results scale linearly with the quantity $(U/E_F)/\delta_o$.) The spatial variation of the electromigration wind force on an impurity is equal to one-half the variation in resistivity for this model.
- Figure 3. STM voltage and LTF plotted against position x near a grain boundary in an aluminum film of thickness 60 a.u. The vertical axis is in units of $E\ell$, where E is the macroscopic electric field and ℓ is the mean free path due to background processes. The grain boundary region is $0 \leq x \leq 4$ a.u. The STM tip is 9.4 a.u. above the film, and the grain boundary potential is 20% of the Fermi energy. The V_{STM} result calculated from a theory which ignores phase coherence between incident and reflected waves (Ref. 1) is indicated by the dashed lines.
- Figure 4. STM voltage (full curves) and LTF (dashed curve) plotted against position near an impurity at the surface of an aluminum film. The STM tip is at height z_o above the surface, and results are shown for $z_o = 2, 4,$ and 6 a.u. The impurity is at the origin, and the coordinate R_{\parallel} is the position of the STM tip along the surface, and measured along a line parallel to the electron wind.

- Figure 5. Upper: the conductance for a bound impurity modeled by local Einstein phonons, with the recoil energy $R = \hbar\omega_0$ and $k_B T = 0$. Lower: The drop of G at different voltages.
- Figure 6. The conductance and its decrease as a function of eV , with $R = 100\hbar\omega_0$ and $k_B T = \hbar\omega_0$. Inset: An enlarged portion showing the stepwise fine structure of the G curve around $eV = R$.
- Figure 7. The conductance and its derivative due to a free impurity with $k_B T = 0.01R$.
- Figure 8. Effective temperatures due to local heating. The solid curve is the effective temperature of non-equilibrium electrons (β_e^{-1}). The dashed curve is the defect temperature (β_d^{-1}) in the presence of a phonon bath. The lattice is at 100K.
- Figure 9. Net atom flux *vs.* electron momentum transfer per collision for hydrogen electro-migration. ($E^* = 0.2$ eV, $T = 300$ K)
- Figure 10. Net atom flux *vs.* electron momentum transfer per collision for hydrogen electro-migration. ($E^* = 0.3$ eV, $T = 300$ K)

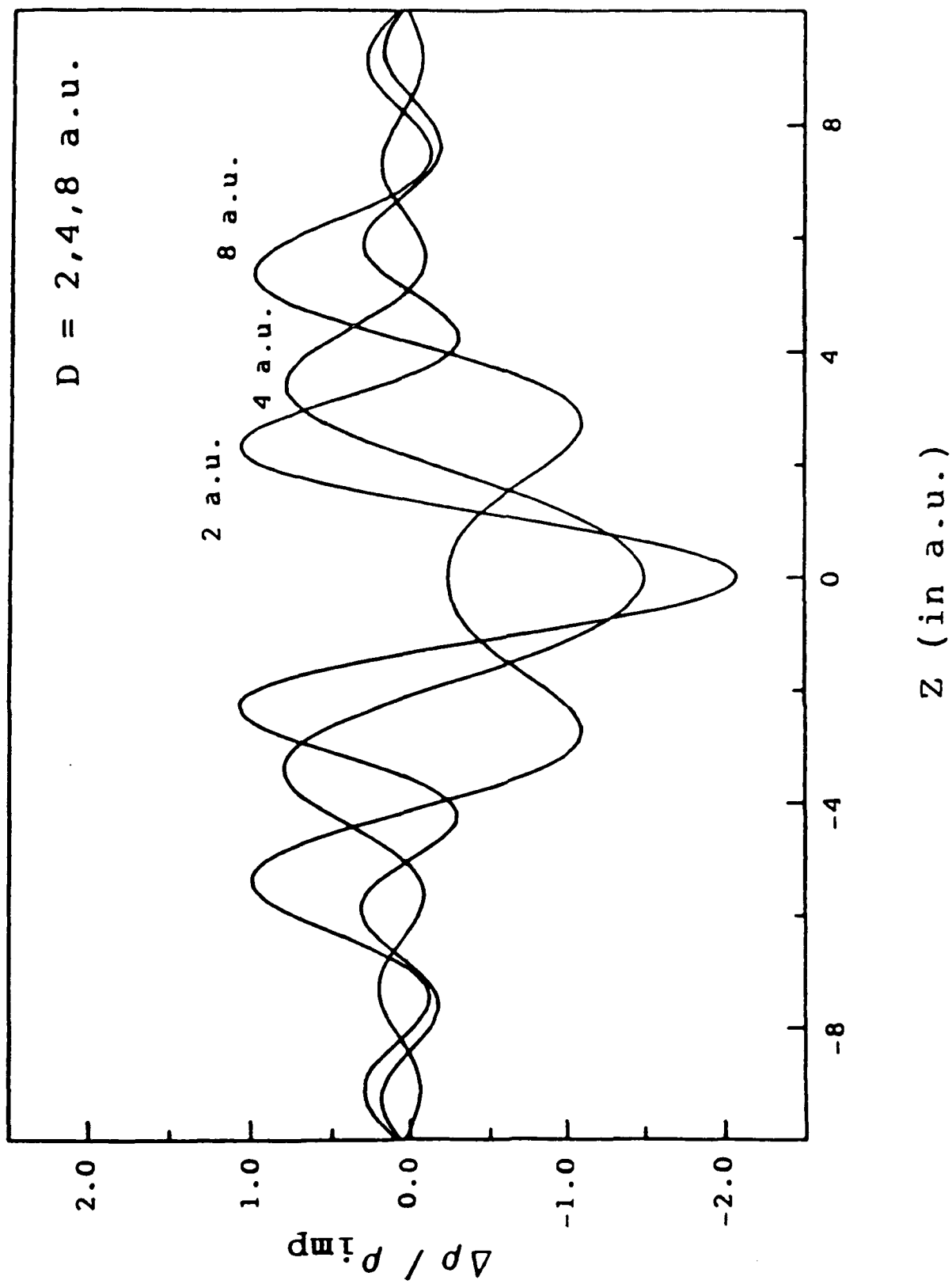


Figure 1. Resistivity variation for an impurity near a grain boundary in aluminum.

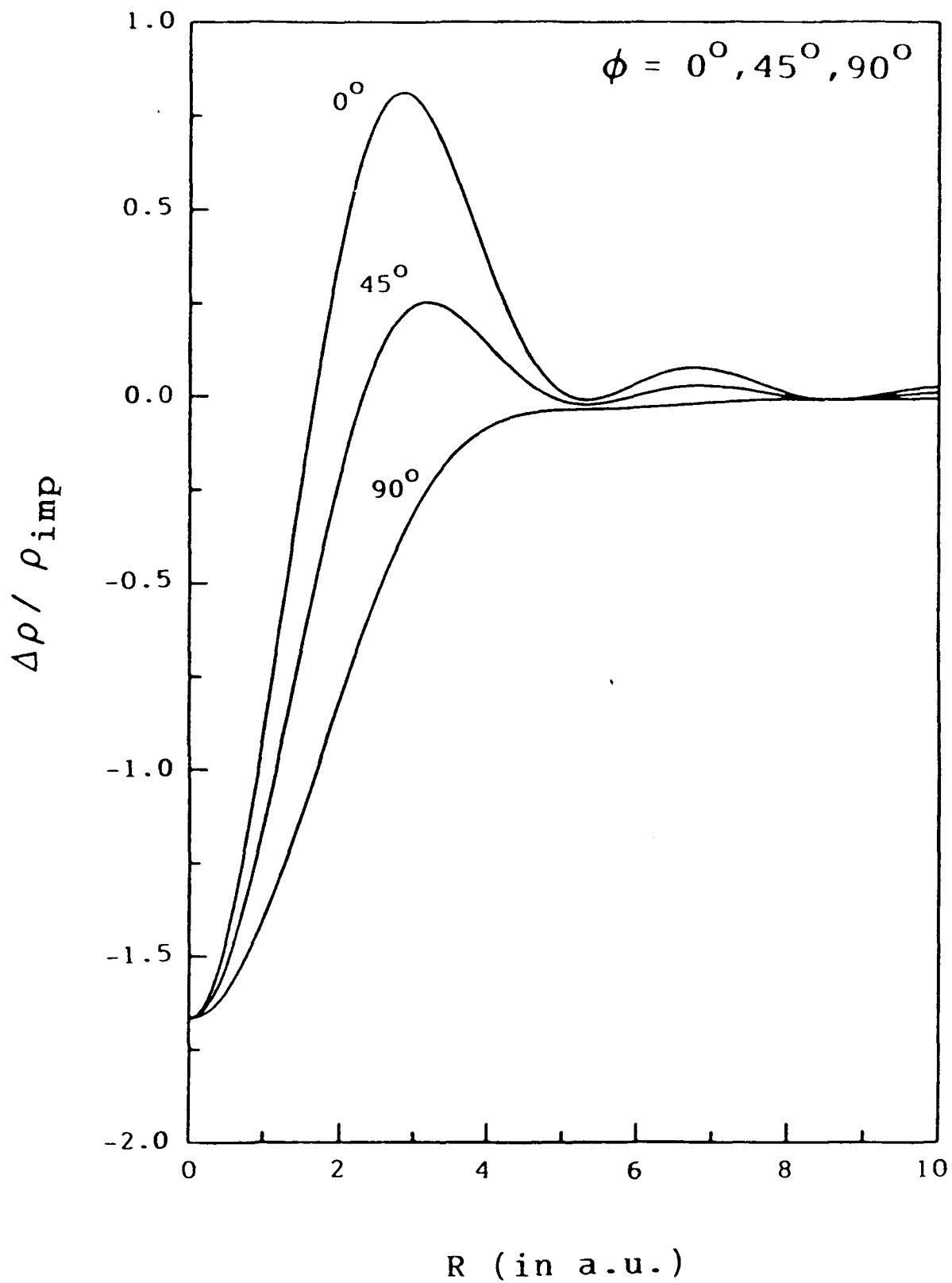


Figure 2. Resistivity variation for an impurity near a dislocation in aluminum.

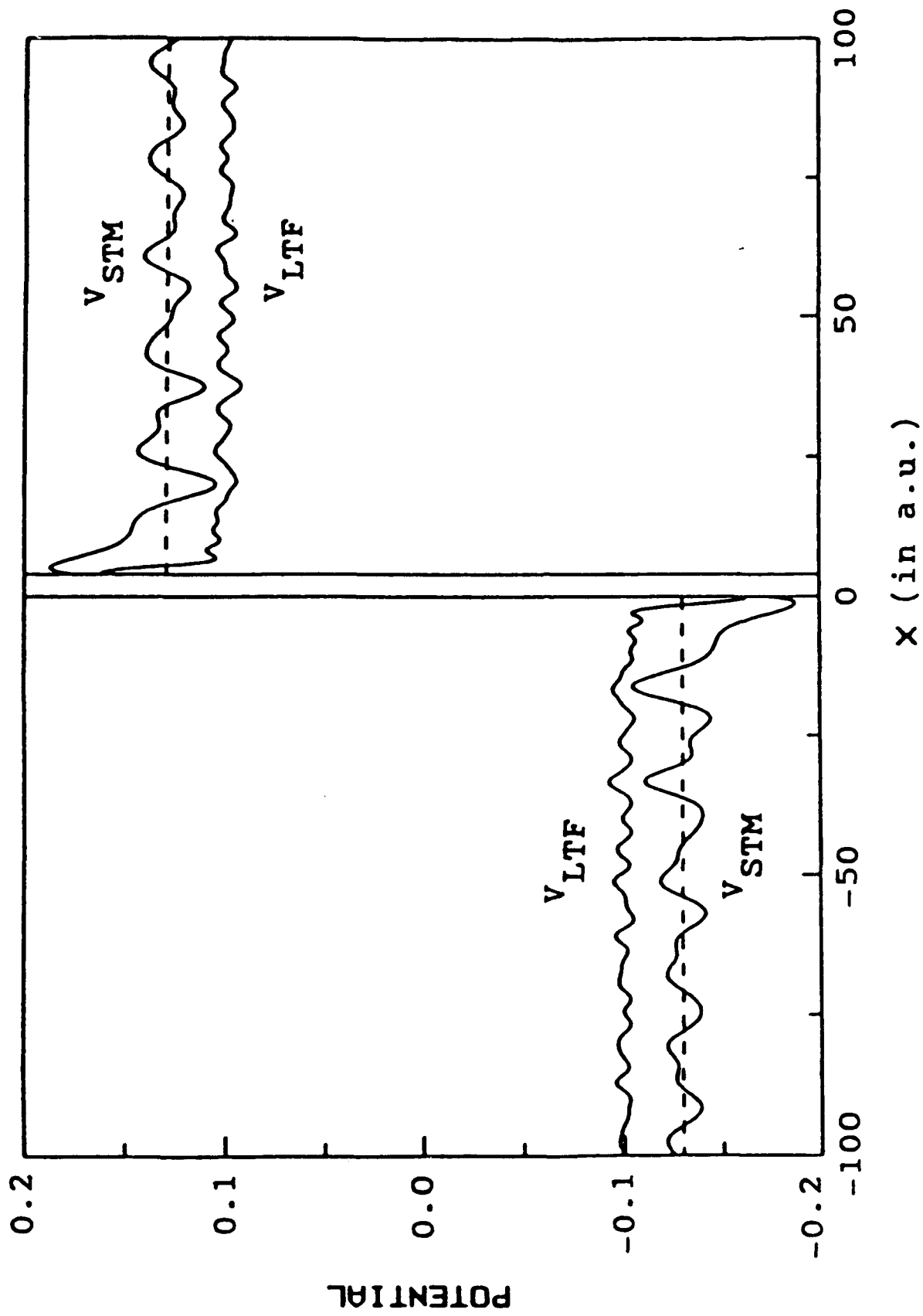


Figure 3. STM voltage and LTF near a grain boundary in aluminum.

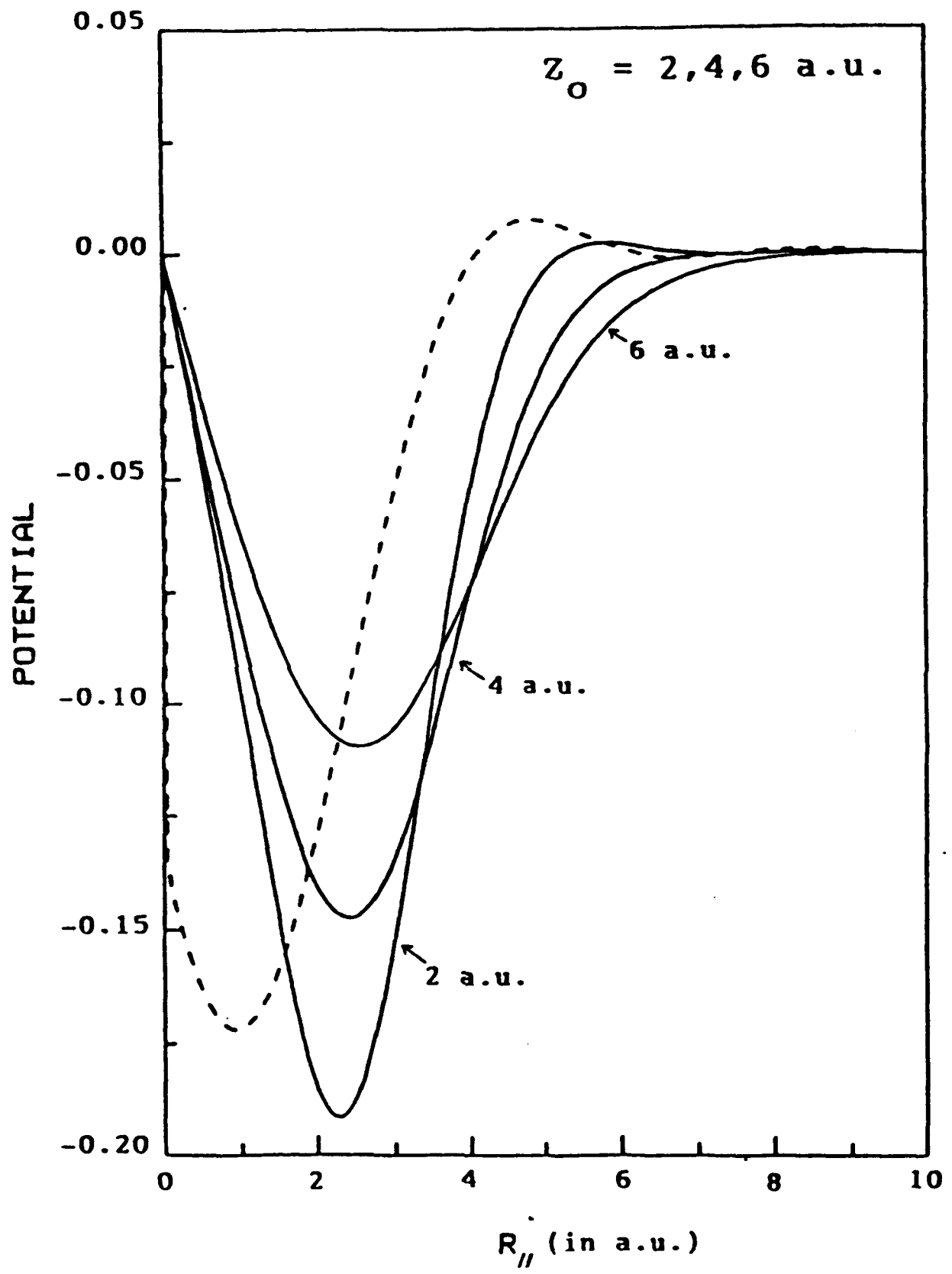


Figure 4. STM voltage and LTF near an impurity at the surface of aluminum.

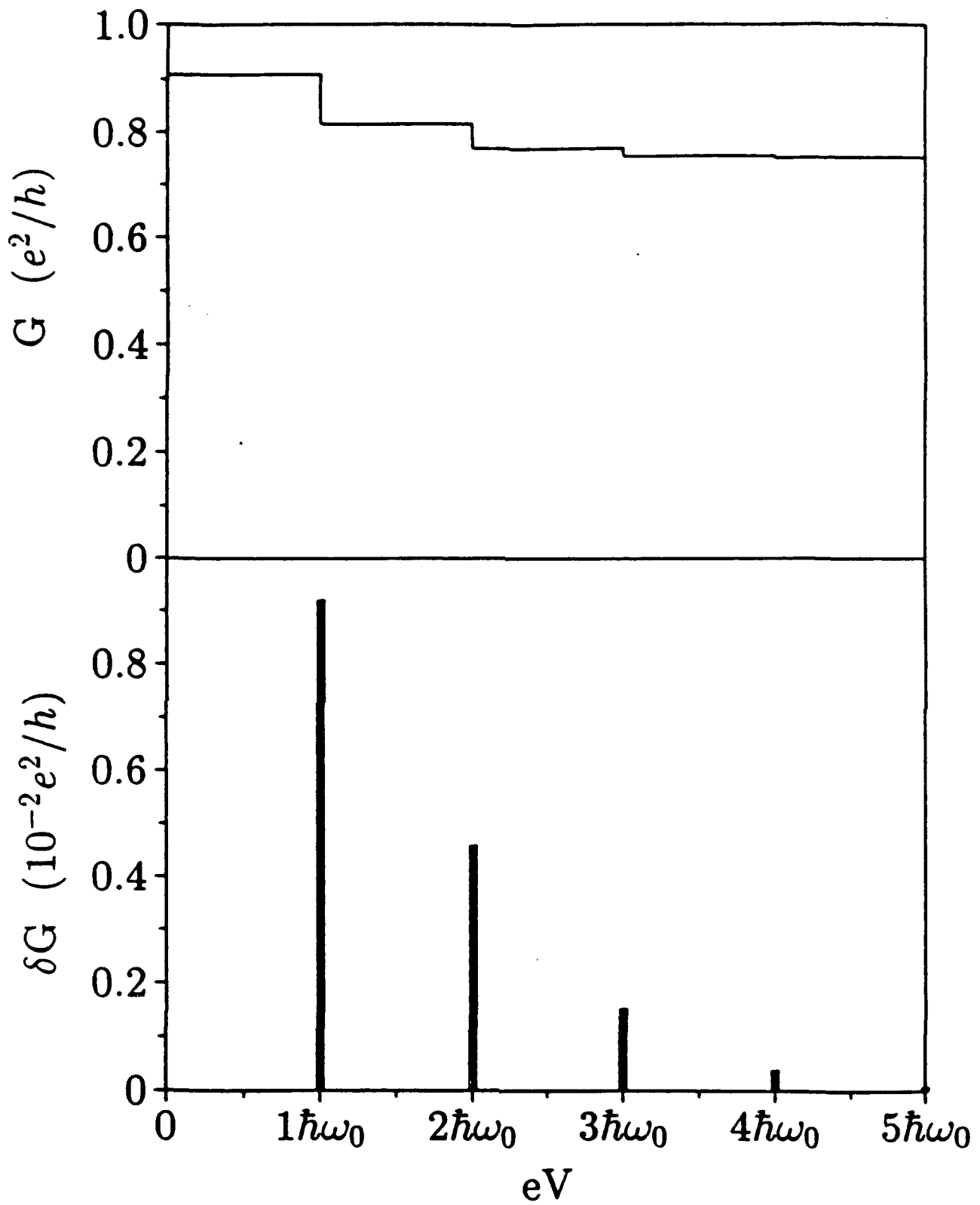


Figure 5. Conductance for a strongly bound impurity in a mesoscopic system.

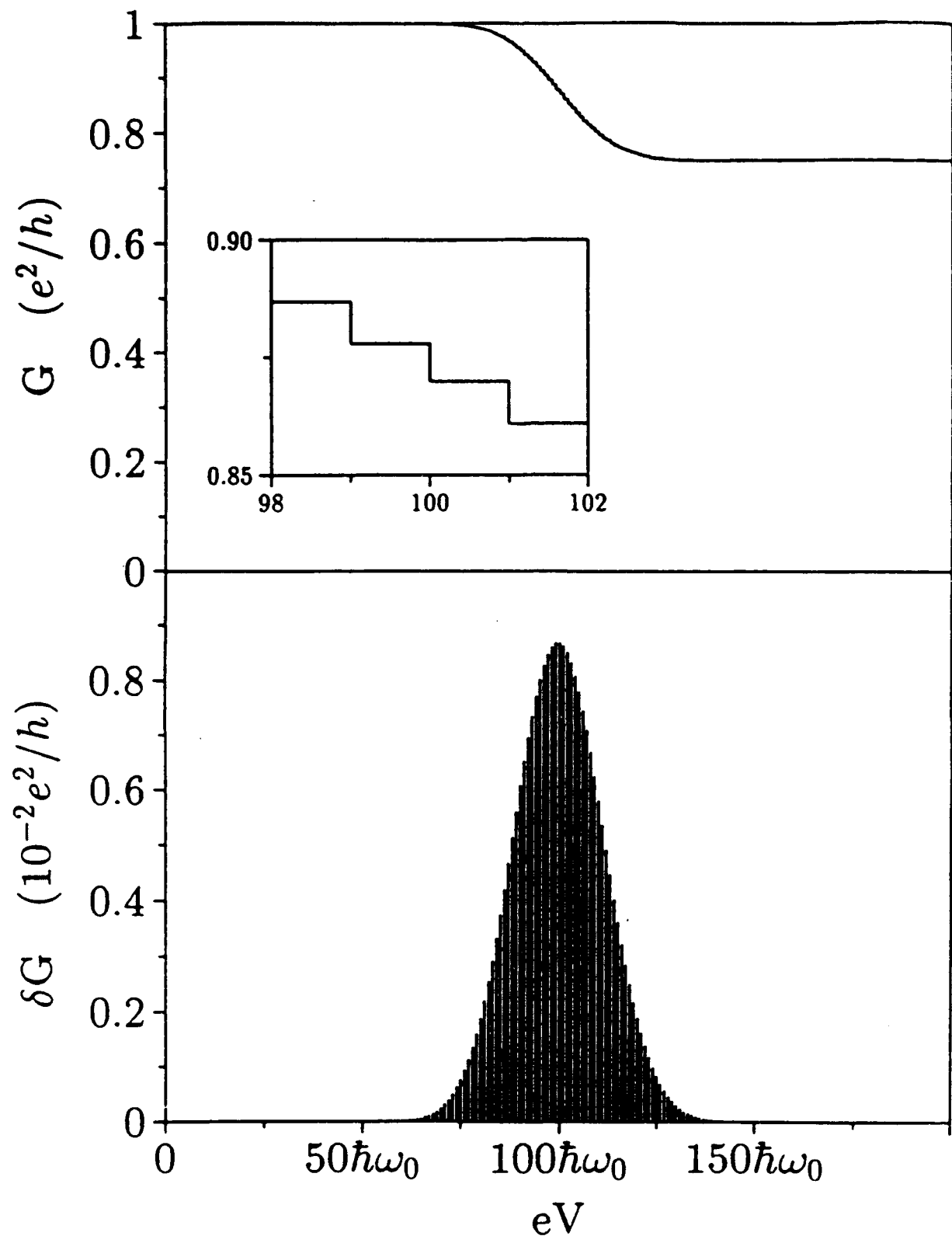


Figure 6. Conductance for a weakly bound impurity in a mesoscopic system.

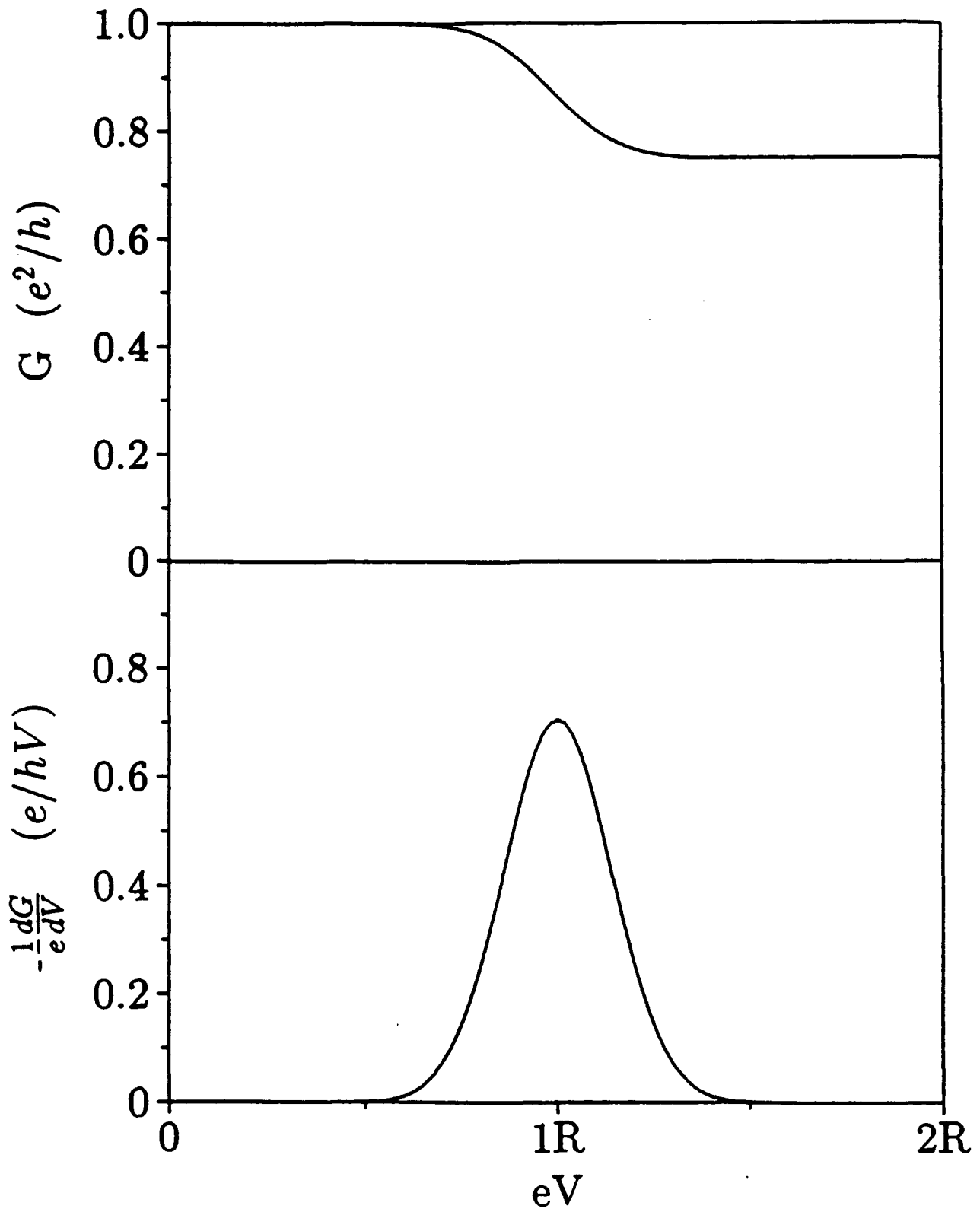


Figure 7. Conductance for a free impurity in a mesoscopic system.

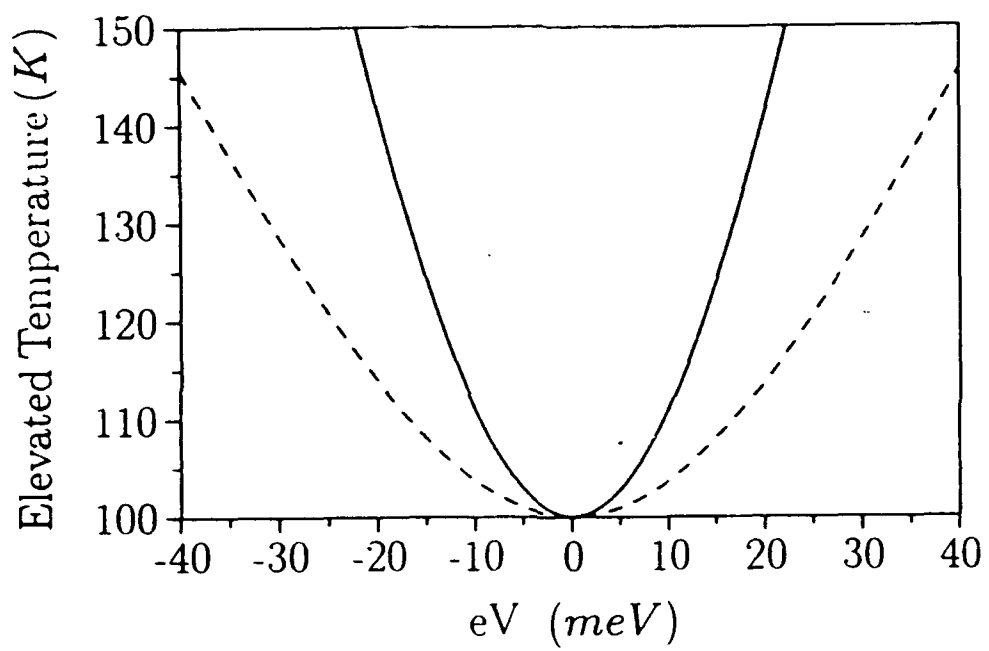


Figure 8. Effective temperatures due to local heating.

HYDROGEN $E^*=0.2\text{eV}$ $T=300\text{K}$

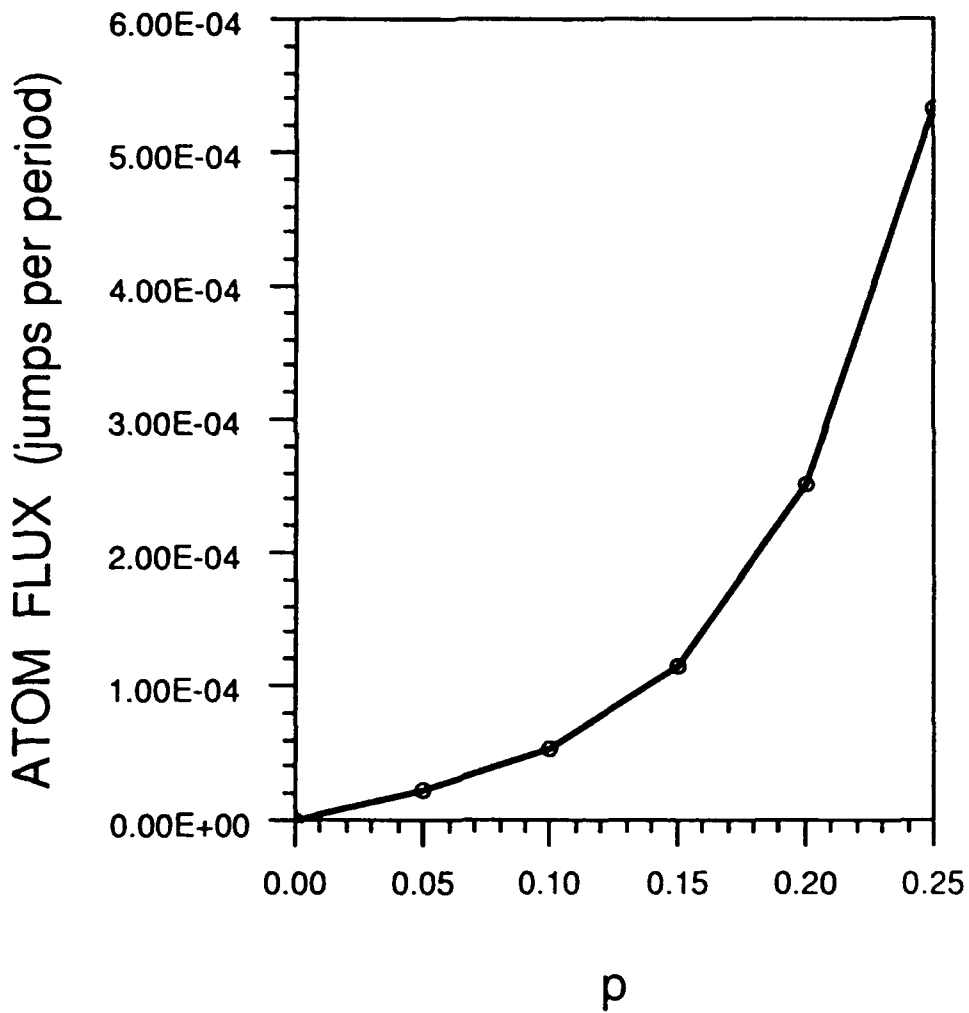


Figure 9. Net atom flux vs. momentum transfer per collision by electrons.

HYDROGEN $E^*=0.3\text{eV}$ $T=300\text{K}$

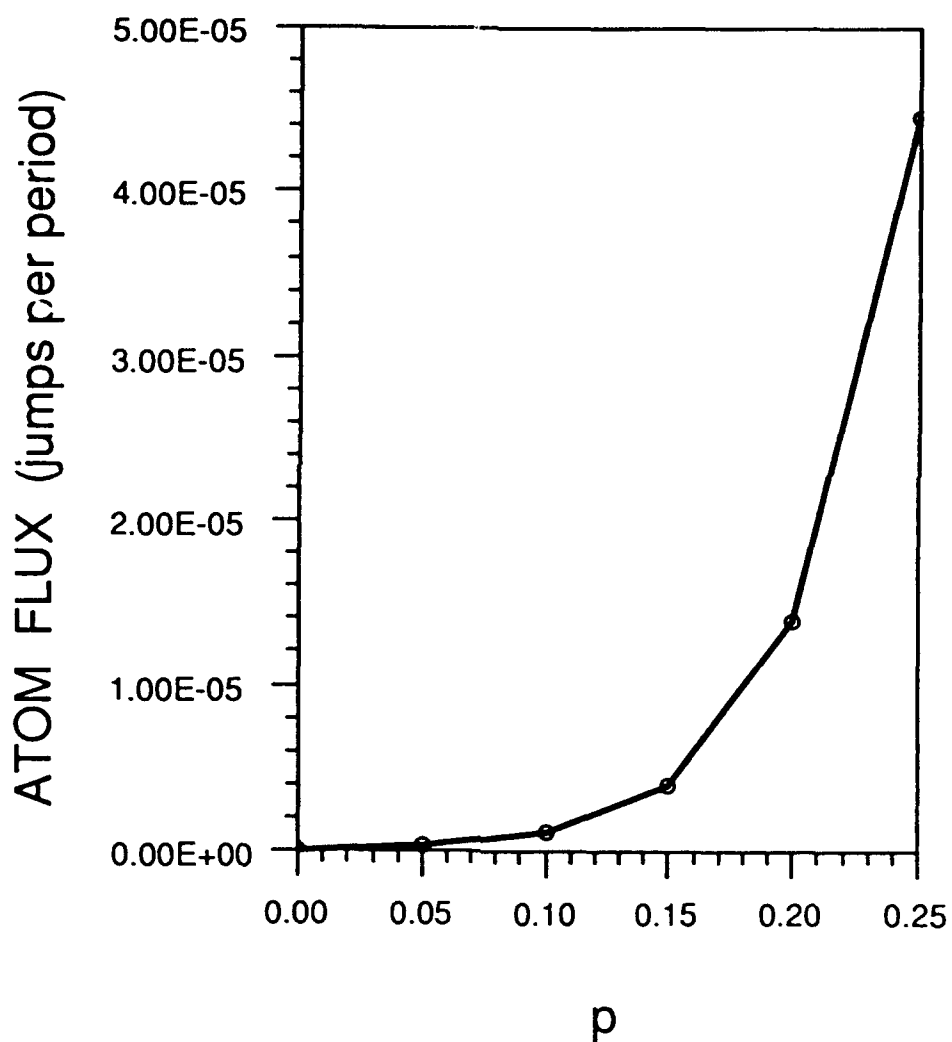


Figure 10. Net atom flux *vs.* momentum transfer per collision by electrons.